Astronomy & Astrophysics manuscript no. Catinella
June 18, 2012
© ESO 2012

arXiv:1206.3059v2 [astro-ph.CO] 15 Jun 2012

The GALEX Arecibo SDSS Survey

VI. Second Data Release and Updated Gas Fraction Scaling Relations

Barbara Catinella[1], David Schiminovich[2], Guinevere Kauffmann[1], Silvia Fabello[1], Cameron Hummels[2], Jenna Lemonias[2], Sean M. Moran[3], Ronin Wu[4], Andrew Cooper[1], and Jing Wang[1]

[1] Max-Planck Institut für Astrophysik, D-85741 Garching, Germany; e-mail: bcatinel@mpa-garching.mpg.de
[2] Department of Astronomy, Columbia University, New York, NY 10027, USA
[3] Department of Physics and Astronomy, The Johns Hopkins University, Baltimore, MD 21218, USA
[4] Commissariat à l'Energie Atomique (CEA), 91191 Gif-sur-Yvette, France

ABSTRACT

We present the second data release from the GALEX Arecibo SDSS Survey (GASS), an ongoing large Arecibo program to measure the HI properties for an unbiased sample of ∼1000 galaxies with stellar masses greater than 10^{10} $M_\odot$ and redshifts $0.025 < z < 0.05$. GASS targets are selected from the Sloan Digital Sky Survey (SDSS) spectroscopic and Galaxy Evolution Explorer (GALEX) imaging surveys, and are observed until detected or until a gas mass fraction limit of a few per cent is reached. This second data installment includes new Arecibo observations of 240 galaxies, and marks the 50% of the complete survey. We present catalogs of the HI, optical and ultraviolet parameters for these galaxies, and their HI-line profiles. Having more than doubled the size of the sample since the first data release, we also revisit the main scaling relations of the HI mass fraction with galaxy stellar mass, stellar mass surface density, concentration index, and NUV−*r* color, as well as the gas fraction plane introduced in our earlier work.

Key words. Galaxies: fundamental parameters – Ultraviolet: galaxies – Radio lines: galaxies – Surveys – Catalogs

1. Introduction

Studies of atomic hydrogen (HI) in galaxies have proved to be of great importance in order to gain insights into some of the main physical processes that drive galaxy evolution (*e.g.*, reviews by Roberts & Haynes 1994 and Sancisi et al. 2008; see also, *e.g.* Walter et al. 2008). In particular, quantifying how the gas content varies with star formation and structural properties of galaxies is of paramount importance for constraining models of galaxy formation. Equally important is to perform such studies on large and unbiased samples of galaxies, in order to obtain results that are truly representative of the local population. In the past few years we have been carrying out the GALEX Arecibo SDSS Survey (GASS; Catinella et al. 2010, hereafter Paper 1), which is designed to provide such a representative sample for massive galaxies, and whose aim is to understand the role played by gas in the transition between blue, star-forming galaxies and red, passively-evolving systems.

GASS uses the Arecibo telescope to measure the HI properties of ∼1000 galaxies with stellar masses greater than 10^{10} $M_\odot$ and redshifts $0.025 < z < 0.05$. For these galaxies, we have homogeneous measurements of structural parameters from the Sloan Digital Sky Survey (SDSS; York et al. 2000), and ultraviolet (UV) photometry from GALEX (Martin et al. 2005) imaging. The availability of multi-wavelength data is essential in order to connect the atomic gas to the other galaxy components, and GASS is optimally configured for follow-up with a range of different telescopes. At $0.025 < z < 0.05$, the angular diameters of GASS galaxies are small enough that accurate total CO fluxes can be obtained in a single pointing[1] of the IRAM 30m telescope in the majority of cases (COLD GASS survey, Saintonge et al. 2011a). Most of the galaxies fit comfortably within a single SDSS frame and GALEX pointing, so that accurate photometry (and hence stellar masses and star formation rates) can be measured. The redshift range does mean, however, that a wide-area blind, shallow survey such as the Arecibo Legacy Fast ALFA (ALFALFA; Giovanelli et al. 2005) survey only detects the most HI-rich galaxies. It has thus been necessary to target galaxies not detected by ALFALFA in order to measure HI mass fractions down to a limit of ∼2-5%.

The combination of GASS on Arecibo, the COLD GASS follow-up on the IRAM 30m telescope (Saintonge et al. 2011a), and long-slit optical spectroscopy on the MMT telescope (Moran et al. 2010, 2012) has yielded a wealth of scientific results. We quantified the scaling relations between atomic and molecular gas fractions and global galaxy properties such as stellar mass, stellar mass surface density $\mu_\star$, NUV−*r* color and concentration parameter (Paper 1; Saintonge et al. 2011a). We showed that galaxies that are unusually HI-rich for their color and $\mu_\star$ have outer disks that are bluer (Wang et al. 2011), younger and more metal poor (Moran et al. 2010, 2012). We also investigated scaling relations between atomic and molecular content and star formation rates (Schiminovich et al. 2010; Saintonge et al. 2011b), and baryonic mass-velocity-size relations (Catinella et al. 2012). Thanks to our multi-wavelength legacy data set, which provides physical information about the stars and atomic, molecular and ionized gas in massive systems, we are gaining significant insight into differences in the evolutionary states of different galaxies, and setting important

[1] The FWHM of the IRAM 30m telescope beam is 22″ at 115 GHz. The optical diameters of GASS galaxies, estimated as twice the Petrosian radius that includes 90% of the *r*-band light from SDSS, are all smaller than 1′, with a mean of 24″.

constraints for theoretical modeling efforts (*e.g.* Fu et al. 2010; Lagos et al. 2011; Davé et al. 2011; Kauffmann et al. 2012).

In this paper we present the second data release of GASS, which marks 50% of the full survey. We use the improved statistics to revisit the gas fraction scaling relations explored in Paper 1, and discuss apparent deviations from linearity that were not evident in the first data release sample, which included ∼20% of the full survey.

All the distance-dependent quantities in this work are computed assuming $\Omega = 0.3$, $\Lambda = 0.7$ and $H_0 = 70$ km s^{-1} Mpc^{-1}. AB magnitudes are used throughout the paper.

2. Sample selection, observations and data processing

Survey design, sample selection, Arecibo observations and data reduction are described in detail in Paper 1, thus we only provide a summary here, including relevant updates.

GASS measures the global HI properties of ∼1000 galaxies, selected uniquely by their stellar mass ($10 < \mathrm{Log}(M_\star/M_\odot) < 11.5$) and redshift ($0.025 < z < 0.05$). The galaxies are located within the intersection of the footprints of the SDSS primary spectroscopic survey, the projected GALEX Medium Imaging Survey and ALFALFA. We defined a GASS *parent sample*, based on SDSS DR6 (Adelman-McCarthy et al. 2008) and the final ALFALFA footprint, which includes 12006 galaxies that meet our survey criteria. The targets for 21cm observations are chosen by randomly selecting a subset of the parent sample which balances the distribution across stellar mass and which maximizes existing GALEX exposure time.

We observe the galaxies with the Arecibo radio telescope until we detect them or until we reach a limit of a few percent in gas mass fraction (defined as $M_{\rm HI}/M_\star$ in this work). Practically, we have set a limit of $M_{\rm HI}/M_\star > 0.015$ for galaxies with $\mathrm{Log}(M_\star/M_\odot) > 10.5$, and a constant gas mass limit $\mathrm{Log}(M_{\rm HI}/M_\odot) = 8.7$ for galaxies with smaller stellar masses. This corresponds to a gas fraction limit 0.015 – 0.05 for the whole sample. Given the HI mass limit assigned to each galaxy (set by its gas fraction limit and stellar mass), we computed the observing time, $T_{\rm max}$, required to reach that value with our observing mode and instrumental setup (see below). We exclude from our sample any galaxies requiring more than 3 hours of total integration time (this effectively behaves like a redshift cut at the lowest stellar masses). As mentioned in Paper 1, we do not re-observe galaxies with good detections already available from ALFALFA and/or the Cornell HI digital archive (Springob et al. 2005, hereafter S05), a homogeneous compilation of HI parameters for ∼9000 optically-selected galaxies.

GASS observations started in March 2008 and are expected to be completed in 2012. Together with the first data release (DR1, Paper 1), the data published in this paper amount to ∼50% of the final survey sample, and were obtained by the end of February 2011, with a total allocation of 572 hours of telescope time (of which ∼13% unusable due to radio frequency interference [RFI] or other technical problems). Arecibo observations are carried out remotely in standard position-switching mode (*i.e.* each observation consists of an on/off source pair, each typically integrated for 5 minutes, followed by the firing of a calibration noise diode). We use the L-band wide receiver and the interim correlator, and record the spectra every second with 9-level sampling. Two correlator boards with 12.5 MHz bandwidth, one polarization, and 2048 channels per spectrum (yielding a velocity resolution of 1.4 km s^{-1} at 1370 MHz before smoothing) are centered at or near the frequency corresponding to the SDSS redshift of the target; two other boards are used for RFI monitoring.

The data reduction, performed in the IDL environment, includes the following steps (for each on/off pair and polarization): Hanning smoothing, bandpass subtraction, RFI excision, and flux calibration. The spectra obtained from each pair are weighted by $1/rms^2$, where rms is the root mean square noise measured in the signal-free portion of the spectrum, and co-added. The two orthogonal linear polarizations are inspected (if present, polarization mismatches are noted in Appendix B) and averaged. The final spectrum is boxcar smoothed, baseline subtracted (we fitted a low-order polynomial, $n \leq 3$, for 80% of our sample; only 6% of the spectra required $5 \leq n \leq 8$), and measured as described in Paper 1. The only difference with respect to DR1 is the estimate of the instrumental broadening correction for the velocity widths. Measured HI linewidths, W_{50}, are corrected as follows:

$$W_{50}^c = \frac{W_{50} - \Delta s}{1 + z} \quad (1)$$

where z is the galaxy redshift and Δs is the instrumental broadening correction, which for DR1 was taken to be the final velocity resolution Δv of the spectrum after smoothing (i.e., between 5 and 21 km s^{-1}). As explained in Catinella et al. (2012, section 2.1), we decided to adopt $\Delta s = 0.5\Delta v$, which is in better agreement with other work (*e.g.* Courtois et al. 2009) and with our own tests on high signal-to-noise GASS HI profiles. Updated values for the DR1 linewidths can be simply obtained from Table 2 of Paper 1 by applying equation 1 to W_{50} (column 7) with $\Delta s = 0.5\Delta v$ (column 5).

3. The second data release

This second data release is incremental over DR1, and includes new Arecibo observations of 240 galaxies. Here we present optical, UV and 21 cm parameters for these objects, and illustrate the main characteristics of the combined DR1+DR2 sample in the following section. The catalogs presented below are available for the combined DR1 and DR2 samples on the GASS website[2].

3.1. SDSS and GALEX data

This section summarizes the quantities derived from optical and UV data used in this paper. All the optical parameters listed below were obtained from Structured Query Language (SQL) queries to the SDSS DR7 database server[3], unless otherwise noted.

The GALEX UV photometry for our sample was reprocessed by us, as explained in Wang et al. (2010) and summarized in Paper 1. Briefly, we produced NUV$-r$ images by registering GALEX and SDSS frames, and convolving the latter to the UV point spread function. The measured NUV$-r$ colors are corrected for Galactic extinction following Wyder et al. (2007), from which we obtained $A_{NUV} - A_r = 1.9807A_r$ (where the extinction A_r is available from the SDSS data base and reported in Table A.1 below). We do not apply internal dust attenuation corrections.

Table A.1 lists the relevant SDSS and UV quantities for the GASS objects published in this work, ordered by increasing right ascension:
Cols. (1) and (2): GASS and SDSS identifiers.

[2] *http://www.mpa-garching.mpg.de/GASS/data.php*
[3] *http://cas.sdss.org/dr7/en/tools/search/sql.asp*

Col. (3): UGC (Nilson 1973), NGC (Dreyer 1888) or IC (Dreyer 1895, 1908) designation, or other name, typically from the Catalog of Galaxies and Clusters of Galaxies (CGCG; Zwicky et al. 1961), or the Virgo Cluster Catalog (VCC; Binggeli et al. 1985).
Col. (4): SDSS redshift, $z_{\rm SDSS}$. The typical uncertainty of SDSS redshifts for this sample is 0.0002.
Col. (5): base-10 logarithm of the stellar mass, $M_\star$, in solar units. Stellar masses are derived from SDSS photometry using the methodology described in Salim et al. (2007) (a Chabrier 2003 initial mass function is assumed). Over our required stellar mass range, these values are believed to be accurate to better than 30%.
Col. (6): radius containing 50% of the Petrosian flux in z-band, $R_{50,z}$, in arcsec.
Cols. (7) and (8): radii containing 50% and 90% of the Petrosian flux in r-band, R_{50} and R_{90} respectively, in arcsec (for brevity, we omit the subscript "r" from these quantities throughout the paper).
Col. (9): base-10 logarithm of the stellar mass surface density, $\mu_\star$, in $\mathrm{M_\odot\ kpc^{-2}}$. This quantity is defined as $\mu_\star = M_\star/(2\pi R_{50,z}^2)$, with $R_{50,z}$ in kpc units.
Col. (10): Galactic extinction in r-band, ext_r, in magnitudes, from SDSS.
Col. (11): r-band model magnitude from SDSS, r, corrected for Galactic extinction.
Col. (12): minor-to-major axial ratio from the exponential fit in r-band, $(b/a)_r$, from SDSS.
Col. (13): inclination to the line-of-sight, in degrees, computed as follows:

$$\cos i = \sqrt{\frac{(b/a)^2 - q_0^2}{1 - q_0^2}}\,, \qquad (2)$$

where b/a is listed in the previous column, and q_0 is the intrinsic axial ratio of a galaxy seen edge-on. We adopt $q_0 = 0.20$ and set the inclination to 90° for galaxies with $b/a < 0.2$ (see Catinella et al. 2012 and discussion therein). However we provide also $(b/a)_r$ to allow different estimates of the inclination.
Col. (14): NUV$-r$ observed color from our reprocessed photometry, corrected for Galactic extinction.
Col. (15): exposure time of GALEX NUV image, T_{NUV}, in seconds.
Col. (16): maximum on-source integration time, $T_{\rm max}$, required to reach the limiting HI mass fraction, in minutes (see § 2). Given the HI mass limit and redshift of each galaxy, $T_{\rm max}$ is computed assuming a 5σ signal with 300 km s^{-1} velocity width and the instrumental parameters typical of our observations (*i.e.*, gain ~10 K Jy^{-1} and system temperature ~28 K at 1370 MHz).

3.2. HI source catalogs

The DR2 sample includes 133 detections and 107 non-detections, for which we provide upper limits below.

The measured HI parameters for the detected galaxies are listed in Table A.2, ordered by increasing right ascension:
Cols. (1) and (2): GASS and SDSS identifiers.
Col. (3): SDSS redshift, $z_{\rm SDSS}$.
Col. (4): on-source integration time of the Arecibo observation, $T_{\rm on}$, in minutes. This number refers to *on scans* that were actually combined, and does not account for possible losses due to RFI excision (usually negligible).
Col. (5): velocity resolution of the final, smoothed spectrum in km s^{-1}.
Col. (6): redshift, z, measured from the HI spectrum. The error on the corresponding heliocentric velocity, cz, is half the error on the width, tabulated in the following column.
Col. (7): observed velocity width of the source line profile in km s^{-1}, W_{50}, measured at the 50% level of each peak. The error on the width is the sum in quadrature of the statistical and systematic uncertainties in km s^{-1}. Statistical errors depend primarily on the signal-to-noise of the HI spectrum, and are obtained from the rms noise of the linear fits to the edges of the HI profile. Systematic errors depend on the subjective choice of the HI signal boundaries (see Paper 1), and are negligible for most of the galaxies in our sample (see also Appendix B).
Col. (8): velocity width corrected for instrumental broadening and cosmological redshift only, $W_{50}{}^c$, in km s^{-1} (see equation 1). No inclination or turbulent motion corrections are applied.
Col. (9): observed, integrated HI-line flux density in Jy km s^{-1}, $F \equiv \int S\ dv$, measured on the smoothed and baseline-subtracted spectrum. The reported uncertainty is the sum in quadrature of the statistical and systematic errors (see col. 7). The statistical errors are calculated according to equation 2 of S05:

$$\epsilon^{stat} = 2\ rms\ \sqrt{1.4 W_{50} \Delta v},$$

where rms is the noise measured in the signal-free part of the spectral baseline (see col. 10), Δv is the velocity resolution of the smoothed spectrum (see col. 5), and the factor 2 accounts for the contribution from uncertainties in the baseline fit (following Schneider et al. 1990).
Col. (10): rms noise of the observation in mJy, measured on the signal- and RFI-free portion of the smoothed spectrum.
Col. (11): signal-to-noise ratio of the HI spectrum, S/N, estimated following Saintonge (2007) and adapted to the velocity resolution of the spectrum. This is the definition of S/N adopted by ALFALFA, which accounts for the fact that for the same peak flux a broader spectrum has more signal.
Col. (12): base-10 logarithm of the HI mass, $M_{\rm HI}$, in solar units, computed via:

$$\frac{M_{\rm HI}}{\mathrm{M_\odot}} = \frac{2.356\times10^5}{1+z}\left[\frac{d_{\rm L}(z)}{\rm Mpc}\right]^2 \left(\frac{\int S\ dv}{\rm Jy\ km\ s^{-1}}\right) \qquad (3)$$

where $d_{\rm L}(z)$ is the luminosity distance to the galaxy at redshift z as measured from the HI spectrum.
Col. (13): base-10 logarithm of the HI mass fraction, $M_{\rm HI}/M_\star$.
Col. (14): quality flag, Q (1=good, 2=marginal, 3=marginal and confused, 5=confused). An asterisk indicates the presence of a note for the source in Appendix B. Code 1 indicates reliable detections, with a S/N ratio of order of 6.5 or higher (this is the same threshold adopted by ALFALFA). Marginal detections have lower S/N, thus more uncertain HI parameters, but are still secure detections, with HI redshift consistent with the SDSS one. The S/N limit is not strict, but depends also on HI profile and baseline quality. As a result, galaxies with S/N slightly above the threshold but with uncertain profile or bad baseline may be flagged with a code 2, and objects with S/N $\lesssim$ 6.5 and HI profile with well-defined edges may be classified as code 1. We assigned the quality flag 5 to eighteen "confused" galaxies, where most of the HI emission is believed to come from another source within the Arecibo beam. For some of the galaxies, the presence of small companions within the beam might contaminate (but is unlikely to dominate) the HI signal – this is just noted in Appendix B. Finally, we assigned code 3 to twelve galaxies, which are both marginal and confused.

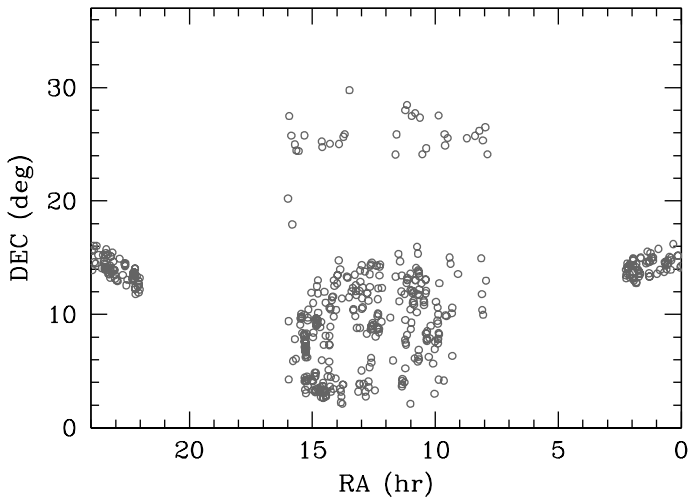

Fig. 1. Sky distribution of the GASS representative sample (480 galaxies).

Table A.3 gives the derived HI upper limits for the non-detections. Columns (1-4) and (5) are the same as columns (1-4) and (10) in Table A.2, respectively. Column (6) lists the upper limit on the HI mass in solar units, Log $M_{\rm HI,lim}$, computed assuming a 5 σ signal with 300 km s^{-1} velocity width, if the spectrum was smoothed to 150 km s^{-1}. Column (7) gives the corresponding upper limit on the gas fraction, Log $M_{\rm HI,lim}/M_\star$. An asterisk in Column (8) indicates the presence of a note for the galaxy in Appendix B.

SDSS images and HI spectra of the DR2 galaxies are presented in Appendix A, organized as follows: HI detections with quality flag 1 in Table A.2 (Figure A.1), marginal detections with quality flag 2 (Figure A.2) and 3 (Figure A.3), confused detections (Figure A.4) and non-detections (Figure A.5). The objects in each of these figures are ordered by increasing GASS number (indicated on the top right corner of each spectrum). The SDSS images show a 1 arcmin square field, *i.e.* only the central part of the region sampled by the Arecibo beam (the half power full width of the beam is ~3.5′ at the frequencies of our observations). Therefore, companions that might be detected in our spectra typically are not visible in the postage stamps, but they are noted in Appendix B. The HI spectra are always displayed over a 3000 km s^{-1} velocity interval, which includes the full 12.5 MHz bandwidth adopted for our observations. The HI-line profiles are calibrated, smoothed (to a velocity resolution between 5 and 21 km s^{-1} for the detections, as listed in Table A.2, or to ~15 km s^{-1} for the non-detections), and baseline-subtracted. A red, dotted line indicates the heliocentric velocity corresponding to the optical redshift from SDSS. In Figures A.1-A.4, the shaded area and two vertical dashes show the part of the profile that was integrated to measure the HI flux and the peaks used for width measurement, respectively.

4. GASS sample properties

Taken together, the first and second GASS data releases include 416 galaxies, of which 232 are HI detections and 184 are non-detections. We will refer to this as the GASS *observed* sample. Because we do not reobserve galaxies with good HI detections already available from either ALFALFA or the S05 archive, this data set lacks the most gas-rich objects, which need to be added back in the correct proportions. By following the procedure described in section 7.2 of Paper 1, we obtained a sample that includes 480 galaxies (of which 296 are detections) and that is representative in terms of HI properties. We will refer to this as the GASS *representative* sample. Notice that, because of the improved statistics compared to DR1, here we use only one such representative sample (as opposed to a suite of 100 realizations, differing for the set of randomly-selected gas-rich galaxies added to the GASS observations).

The sky distribution of the representative sample is shown in Figure 1. We restricted the observations as much as possible to the two declination intervals from +4° to +16° and from +24° to +28°, for which ALFALFA catalogs were available to us in advance of publication (Haynes et al. 2011). The uneven right ascension distribution is the result of telescope allocation, which favored small observing session at LST intervals less oversubscribed (such as 14−16 hours).

The HI properties of the detected galaxies are illustrated in Figure 2 for both observed (blue histograms) and representative (dotted) samples. The solid black histogram in the top left panel shows the redshift distribution for the full representative sample, using the SDSS redshifts for the non-detections. As for the DR1 sample presented in Paper 1, the distribution of corrected velocity widths (which have not been deprojected to edge-on view) peaks near 300 km s^{-1}, which is the value that we assume to compute upper limits for the HI masses of the non-detections, and to estimate $T_{\rm max}$ in Table A.1.

Figure 3 presents the stellar mass (a) and NUV−r color (c) distributions for the observed (black histogram) and representative (dotted) samples. The corresponding distributions for the non-detections are shown as hatched green histograms. The stellar mass histogram is almost flat by survey design, as we wish to obtain similar statistics in each bin in order to perform comparisons at fixed stellar mass. As already noted in Paper 1, non-detections span the entire range of stellar masses, but they are concentrated in the red portion of the NUV−r space. The detection fraction, *i.e.* the ratio of detected galaxies to total, is plotted as a function of stellar mass in (b). The detection fraction is close to 70% for $M_\star < 10^{10.7}$ M$_\odot$, and drops to ~30% in the highest stellar mass bin.

The NUV−r color-stellar mass diagram shown in Figure 4 combines the information contained in Figures 3a and 3c. In order to clearly indicate the loci of the blue cloud and red sequence, we use the GASS *parent sample* mentioned in § 2, which is the complete set of 12,006 galaxies that meet our selection criteria. The locations of these galaxies in the diagram are shown by the grayscales; the red sequence peaks at NUV−r~5.5 mag, and the blue cloud is mostly confined to NUV−r< 3.5 mag. The results for the GASS representative sample are indicated by red and green symbols. GASS non-detections are almost entirely confined to the red sequence. We note that, because we select targets with an approximately flat stellar mass distribution (see Section 2 and Fig. 3), we oversample the high stellar mass galaxies, which are more rare in a volume-limited survey. Hence the distribution of our representative sample in the color-stellar mass diagram is somewhat offset toward higher $M_\star$ values compared to that of the GASS *parent sample*.

5. Gas fraction scaling relations

The updated versions of the scaling relations investigated in Paper 1 are presented in Figures 5 and 6. We describe the figures first, and discuss them together afterward.

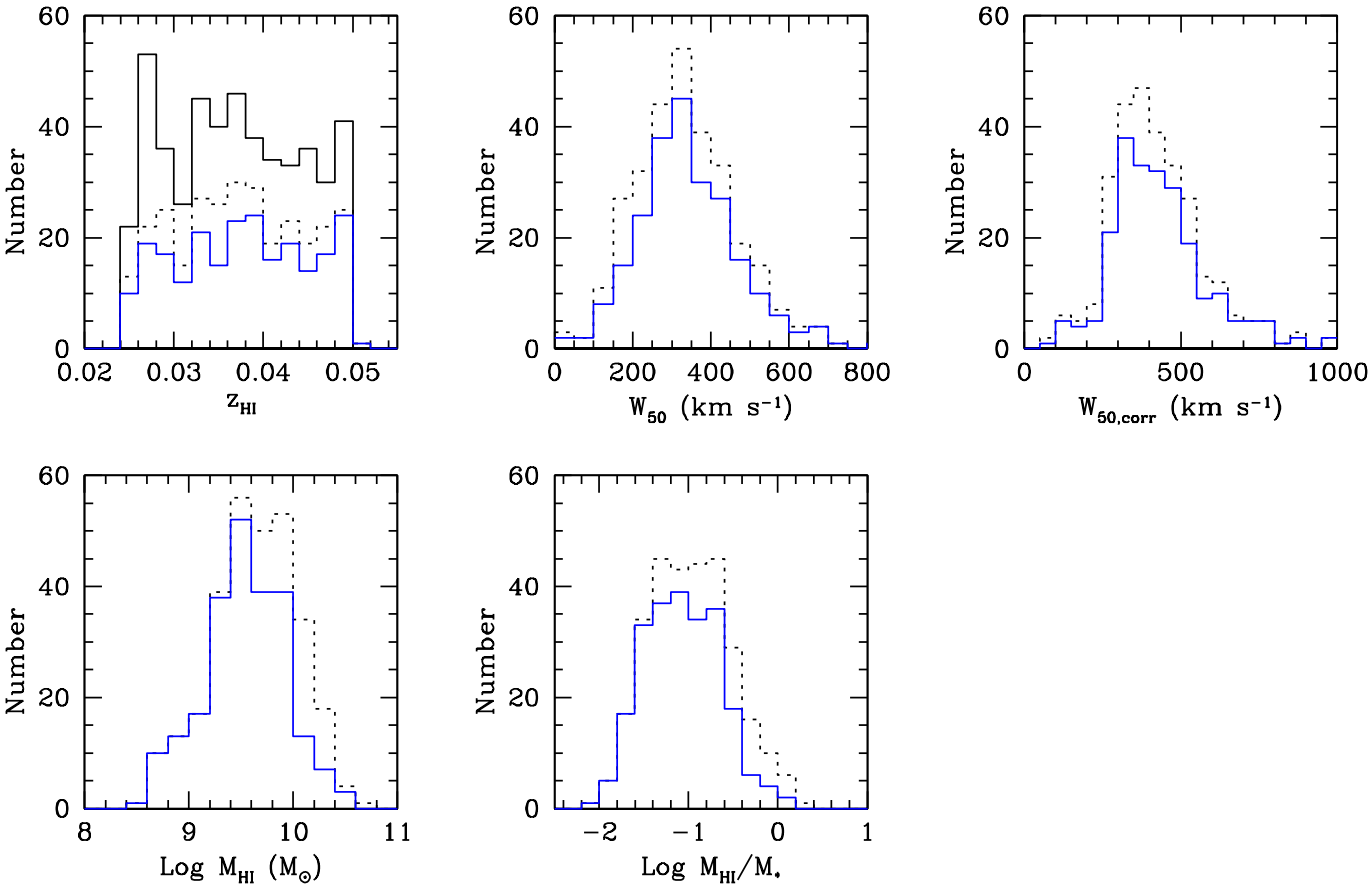

Fig. 2. Distributions of redshifts, velocity widths, velocity widths corrected for inclination, HI masses and gas mass fractions for the galaxies with HI detections from GASS (blue histograms, 232 galaxies). Dotted histograms correspond to the representative sample, which includes gas-rich objects from ALFALFA and/or S05 archive (see text). The solid black histogram in the top left panel shows the distribution of SDSS redshifts for the full sample (*i.e.* including the non-detections).

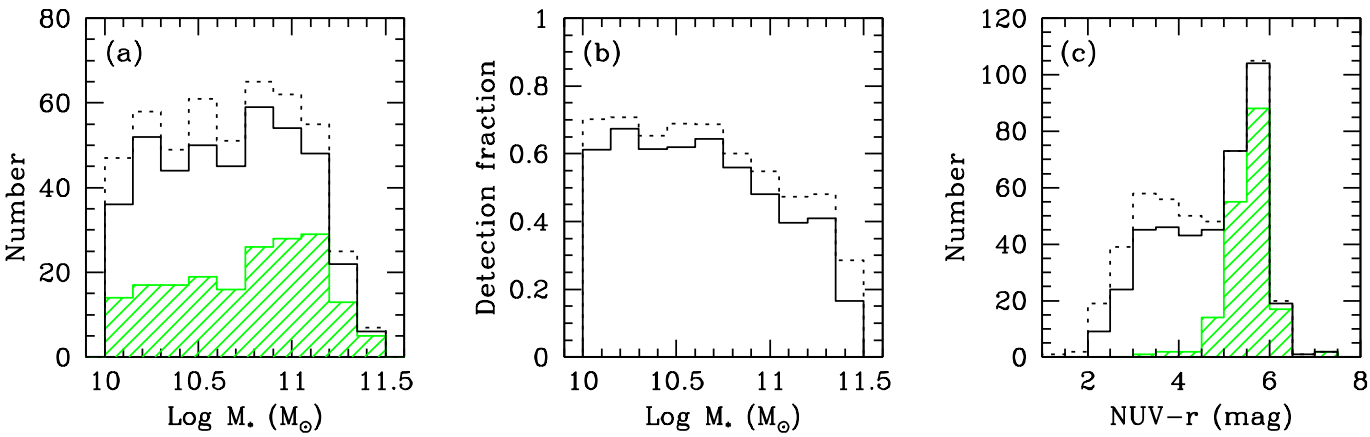

Fig. 3. Stellar mass (a) and observed NUV−r color (c) distributions for the GASS observed sample (solid). Hatched histograms indicate the corresponding distributions for the non-detections. The detection fraction (*i.e.*, the ratio of detections to total) is shown as a function of stellar mass in (b). The dotted histograms in all panels show the distributions for the representative sample (see text).

Clockwise from the top left, Figure 5 shows how the gas mass fraction $M_{\rm HI}/M_\star$ depends on stellar mass, stellar mass surface density, observed NUV−r color and concentration index for the GASS representative sample. Red circles and green upside-down triangles indicate HI detections and non-detections (plotted at their upper limits), respectively. ALFALFA detections of galaxies in the parent sample (1102 objects in total), whose HI masses have been computed consistently with GASS ones from the fluxes tabulated by Haynes et al. (2011), are shown as gray

dots for comparison. Dotted lines in each panel are linear fits to the detections, which we use only to quantify the scatter σ.

The average values of the gas fraction are plotted as a function of the same quantities in Figure 6. Gray and green symbols reproduce individual GASS detections and non-detections, respectively, from Figure 5. The averages are computed including the non-detections, whose HI masses were set either to their upper limits (green circles) or to zero (red circles). As in Paper 1, these averages are weighted in order to compensate for the flat stellar mass distribution of the GASS sample, using the volume-limited parent sample as a reference. Briefly, we binned both the parent sample and the GASS representative sample by stellar mass (with a 0.2 dex step), and used the ratio between the two histograms as a weight. Error bars indicate the standard deviation of the weighted averages. Lastly, weighted median values of the gas fraction, calculated using upper limits for the HI masses of the non-detections, are plotted as green triangles. The values of weighted average and median gas fractions shown in this figure are listed in Table 1 for reference.

These results are consistent with our previous findings (see also Fabello et al. 2011 and Cortese et al. 2011), and show that:
– The gas fraction of GASS detections is a decreasing function of stellar mass, stellar mass surface density, and NUV$-r$ color. The scatters around the linear fits to these relations are unchanged with respect to DR1 (σ = 0.39, 0.36 and 0.33 dex, respectively), despite the fact that the sample size has more than doubled (from ~200 to 480 galaxies).
– The strongest correlation is with observed NUV$-r$ color (Pearson correlation coefficient $r = -0.69$); the average $M_{\rm HI}/M_\star$ decreases from 73% to 2% from the bluest to the reddest galaxies. The decrease quoted in Paper 1 was smaller because, due to poorer statistics, we did not have enough observations below NUV$-r$= 2.9 mag to compute an average gas fraction. Given the link between star formation rate and gas content, the strong correlation between NUV$-r$ and gas fraction is expected, though as we note further below and in the next section, departures from a tight, linear correlation may result from contributions to UV light from an older population, or alternatively, diminished UV from dust attenuation.
– The weakest correlations are with stellar mass ($r = -0.53$) and concentration index ($r = -0.37$; the scatter is $\sigma = 0.43$ dex, it was 0.45 dex for the DR1 sample). In both cases, the difference between average and median gas fractions points to the presence of significant tails of galaxies with small values of $M_{\rm HI}/M_\star$. The relation between gas fraction and stellar mass surface density has a correlation coefficient $r = -0.62$.
– All the non-detections have stellar mass surface density $\mu_\star > 10^{8.5}$ M$_\odot$ kpc^{-2}. The average gas fractions are insensitive to the way we treat the non-detections, except for the very most massive, dense and red galaxies.
– In the GASS stellar mass and redshift intervals, ALFALFA only detects the bluest, most gas-rich objects.

With our improved statistics, the relation between gas fraction and NUV$-r$ color *for the detections* now seems to show a break at NUV$-r$~3.5 mag, which corresponds approximately to the upper envelope of the blue sequence (see Figure 4). The galaxies with the highest gas fractions systematically lie above the linear fit to the detections (Figure 5). This can be seen also in Figure 6, if we focus on the bins that are not dominated by the non-detections. Interestingly, including the non-detections in the computation of the average gas fractions restores the linearity of the relation with NUV$-r$ color. This agrees with the results based on the Herschel Reference Survey (HRS; Boselli et al. 2010) sample, which is more local and thus probes significantly lower gas fractions than GASS. The HRS $M_{\rm HI}/M_\star$ versus NUV$-r$ relation does not show any evidence for a change of slope (see Fig. 1 of Cortese et al. 2011), but only an increase of scatter outside the blue sequence, which we observe as well. We will come back to this point in the next section.

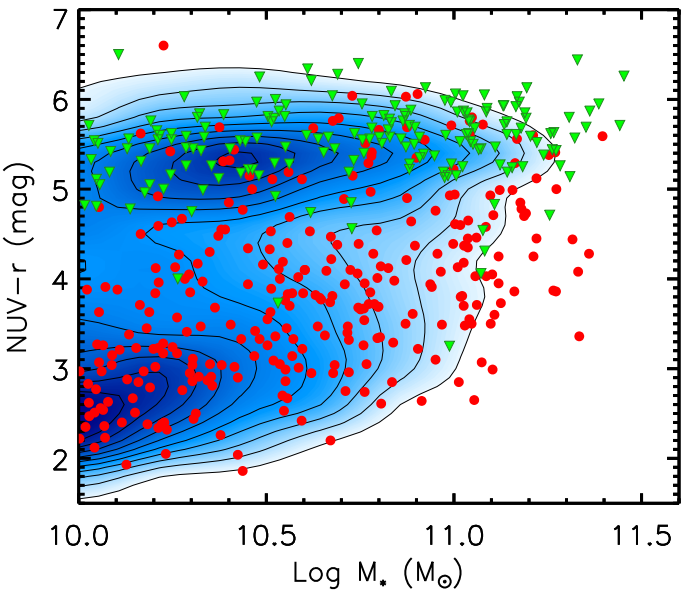

Fig. 4. Color-stellar mass diagram for the GASS *parent sample*, the super-set of ~12,000 galaxies that meet the survey criteria (grayscales). Red circles and green upside-down triangles indicate HI detections and non-detections, respectively, from the representative sample.

6. Gas fraction plane

In Paper 1 we introduced the *gas fraction plane*, a relation between gas mass fraction and a linear combination of NUV$-r$ color (which is a proxy for star formation rate per unit stellar mass) and stellar mass surface density, which can be used to define what is "HI normalcy" for local massive, star-forming galaxies. As discussed by Zhang et al. (2009), such a relation is a direct consequence of the Kennicutt-Schmidt global star formation law (Schmidt 1963; Kennicutt 1998) if one assumes that star formation and gas densities are computed over the same spatial area — thus it is physically motivated. Figure 7a shows the result for the GASS representative sample. We remind the reader that the best fit relation is obtained following Bernardi et al. (2003) (*i.e.*, this is the solution that minimizes the scatter on the y coordinate, and therefore it is equivalent to a direct fit), and that only HI detections (red circles) are used. The coefficients of the fit (reported on the x axis of the figure) and the rms scatter in Log $M_{\rm HI}/M_\star$, 0.319 dex, are almost unchanged with respect to the DR1 solution, showing that the 20% survey sample was indeed representative. The Pearson correlation coefficient for the relation shown in Figure 7a is $r = -0.71$.

We note that Li et al. (2012) presented a slightly different solution for this gas fraction plane (see their Fig. 2), obtained by weighting each galaxy by the mass-dependent selection function of GASS. However, the weights make negligible difference to the result (they obtain Log $M_{\rm HI}/M_\star = -0.322$ Log $\mu_\star - 0.234$ NUV$-r$+2.817, with identical scatter, 0.32 dex).

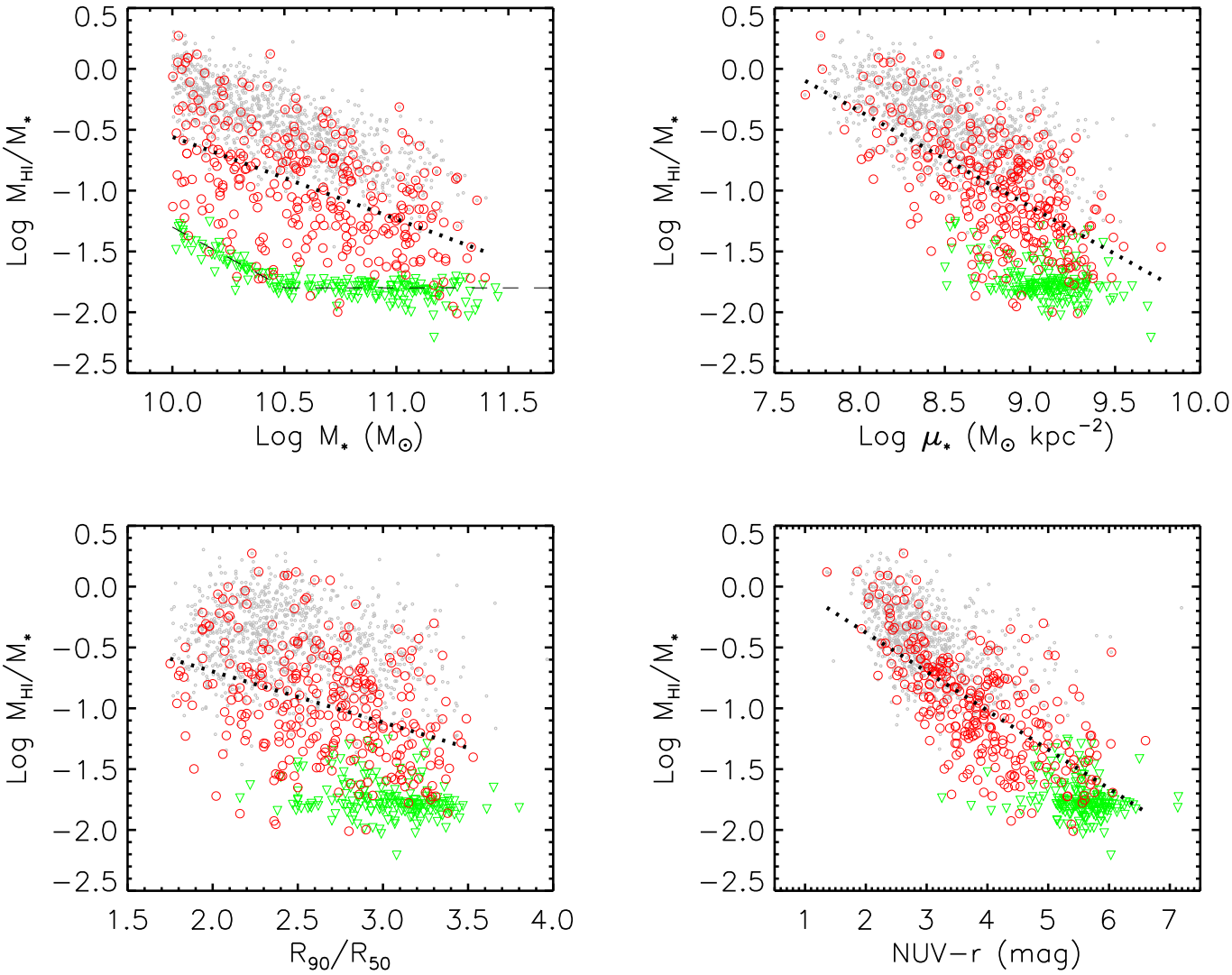

Fig. 5. The HI mass fraction of the GASS sample is plotted here as a function of stellar mass, stellar mass surface density, concentration index, and observed NUV−r color. Red circles and green triangles represent detections and non-detections, respectively. For comparison, we also show the full set of ALFALFA galaxies meeting the GASS selection criteria that have been cataloged to date (gray). The dashed line on the top-left panel indicates the HI detection limit of the GASS survey. Dotted lines in each panel are linear fits to the HI detections only.

Our gas fraction plane is also consistent with the one based on the HRS sample, when this is restricted to the HI-normal galaxies (*i.e.*, when HI-deficient systems in the Virgo cluster are excluded; see Cortese et al. 2011). This agreement is a non-trivial result, given the different selection criteria and data sets of the two surveys. Notice however that the scatter of the HRS plane is smaller (0.27 dex, see below).

As can be seen in Figure 7a, the highest gas fraction galaxies lie systematically above the mean relation, indicated by a dashed line. This is the same deviation from linearity discussed for the $M_{\rm HI}/M_\star$ versus NUV−r relation in the previous section. As already noted, the apparent break of the gas fraction-color relation seen for the HI detections is linked to the gas fraction limit of GASS. Indeed the break effectively disappears when non-detections are included in the averages, and a similar discontinuity is not seen for the HRS sample, which probes significantly lower gas fractions.

Because the gas fraction plane is computed using only detections, its validity breaks down in the region where the contribution of the non-detections becomes important. Thus, a more reliable solution for the plane can be obtained by using only galaxies with NUV−r≤ 4.5 mag, where we have virtually only detections (this is a conservative threshold based on the inspection of Figure 3c). This cut has the additional advantage of excluding a region of parameter space that is problematic for two reasons. First, outside the blue sequence, the UV emission might not be physically associated to the HI, but might trace a more evolved stellar population, and thus NUV−r might no longer be a good proxy for specific star formation rate (see also O'Connell 1999; Boselli et al. 2005; Cortese & Hughes 2009). This increases the scatter of the gas fraction-color relation outside the blue sequence. Second, both NUV−r and $\mu_\star$ saturate, *i.e.* they never exceed NUV−r~6 mag and Log $\mu_\star$~9.5 $M_\odot$ kpc^{-2}. This will introduce an apparent non-linearity in the relations involving gas fraction regardless of HI content.

The gas fraction plane computed using only galaxies with NUV−r≤ 4.5 mag is shown in Figure 7b: the relation becomes more linear, but clearly the scatter of the redder galaxies (shown

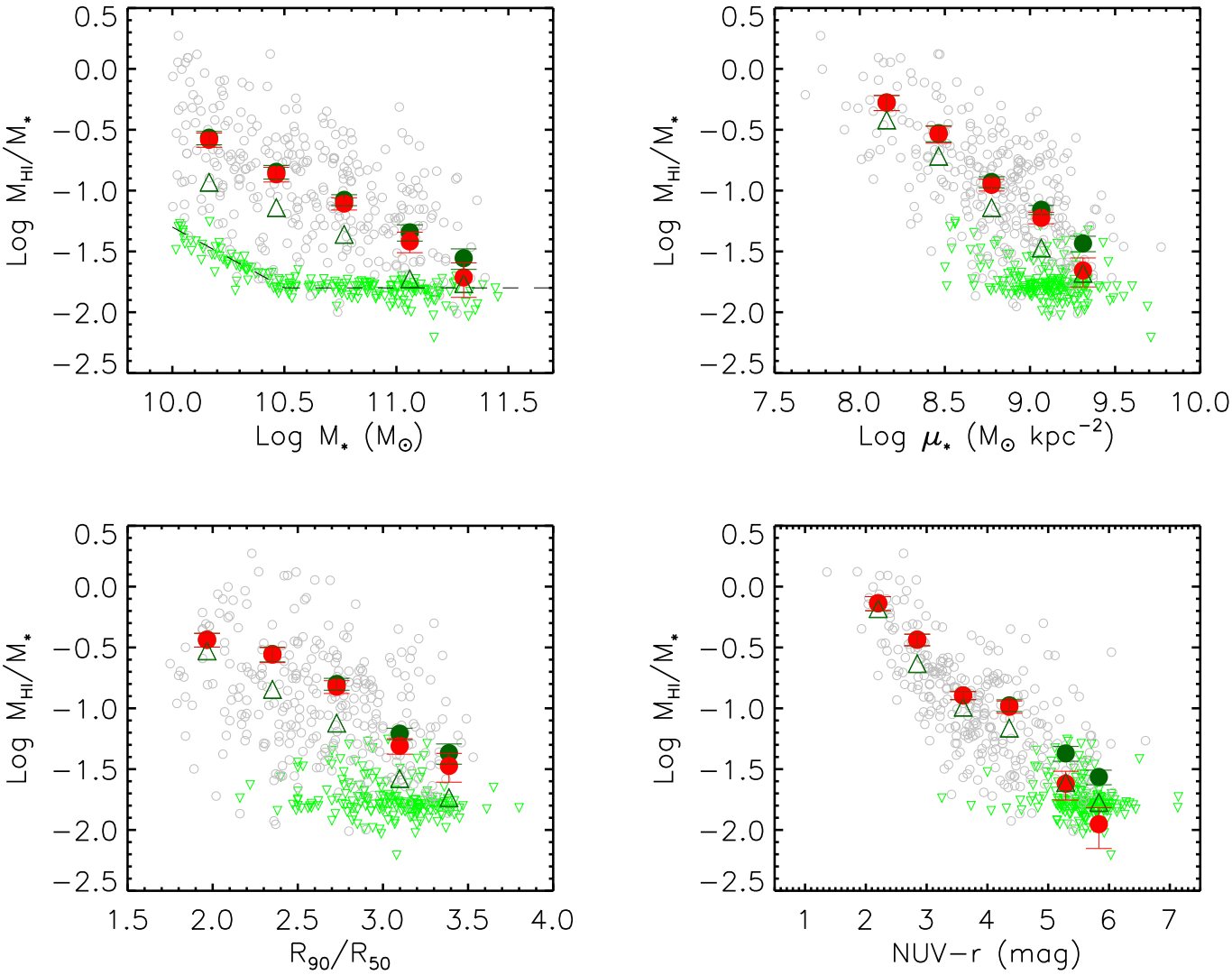

Fig. 6. Average trends of HI mass fraction as a function of stellar mass, stellar mass surface density, concentration index and observed NUV−r color for the representative sample. In each panel, large circles indicate weighted average gas fractions (see text). These were computed including the non-detections, whose HI mass was set to either its upper limit (dark green) or to zero (red). Green triangles are weighted medians. Only averages based on at least 8 galaxies are shown. These results are listed in Table 1. GASS data from Figure 5 are shown in gray and green (for detections and non-detections, respectively). The dashed line in the first panel shows the HI detection limit of the GASS survey.

in gray) increases. Importantly, the main outliers remain the same. The scatter of the plane in Figure 7b is 0.29 dex over the subset of galaxies used for its computation (and 0.32 dex when all detections are included), which better agrees with the scatter of the HRS plane (0.27 dex).

We note that the GASS DR1 sample included too few galaxies on the top right corner of the plane to notice a clear deviation for the galaxies with the highest gas fractions. Our improved statistics allows us to look now into second order corrections, such as the one suggested above. Naturally, one has to keep in mind that the relation used to predict gas fractions has only a statistical validity, and should not be trusted for an individual galaxy.

Another approach to obtain a better prediction for the gas fractions of the galaxies with the highest values of $M_{\rm HI}$ and/or $M_{\rm HI}/M_\star$ is to correct the non-linearity by adding degrees of freedom when fitting the plane (although this is no longer physically justified by the Kennicutt-Schmidt star formation law). As shown by Wang et al. (2011), gas-rich galaxies tend to have bluer-than-average outer disks. Thus, Li et al. (2012) advocate that a new gas fraction estimator that includes two additional parameters, stellar mass and $g-i$ color gradient (defined as the difference between outer and inner $g-i$ color), yields a better fit to the HI-rich galaxies. However, over the GASS stellar mass regime, the scatter decreases very little (from 0.32 to 0.31 dex, see their Figure 2).

7. Conclusions

This paper presents the second data release of GASS, an ongoing large Arecibo program to measure HI parameters for ~1000 massive galaxies, selected from the SDSS spectroscopic and GALEX imaging surveys. This release is incremental over the first one (Paper 1), and includes new HI observations for 240 galaxies. The representative sample presented here, which was obtained by adding the correct proportion of HI-rich objects de-

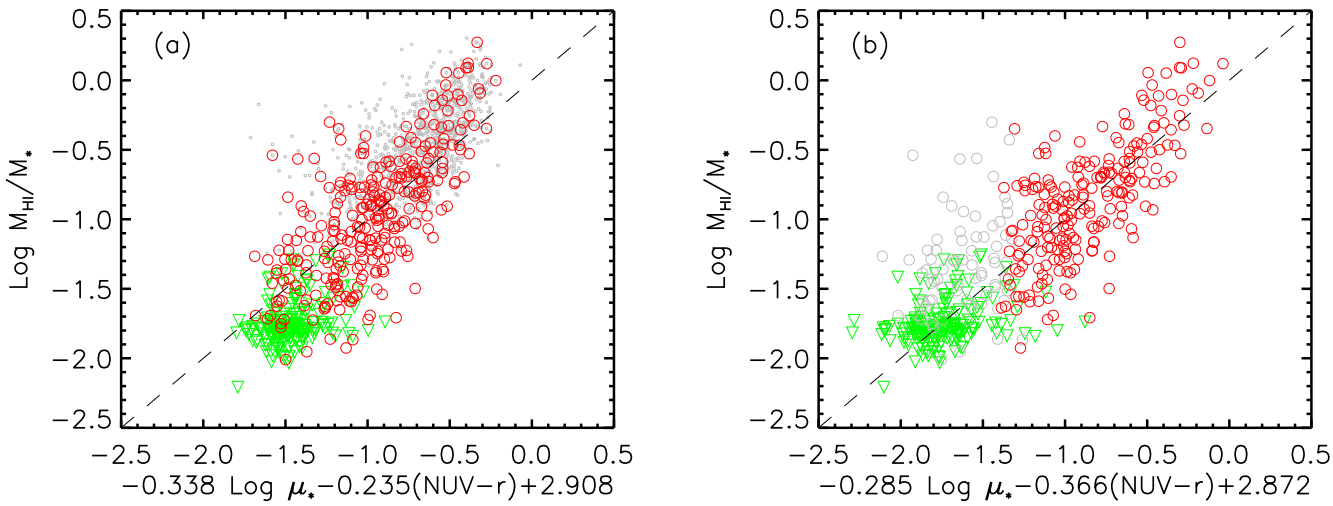

Fig. 7. Gas fraction plane, a relation between HI mass fraction and a linear combination of stellar mass surface density and observed NUV−r color. (a) Relation obtained using all the HI detections in the GASS representative sample (red circles). The symbols are the same as those in Fig. 5. (b) Relation obtained using only the subset of detected galaxies with NUV−r≤ 4.5 mag (red circles). Gray circles and green upside-down triangles indicate the remaining HI detections and the non-detections, respectively.

Table 1. Weighted Average and Median Gas Fractions

x	$\langle x \rangle$	$\langle M_{HI}/M_\star \rangle$ (average)[a]	$\langle M_{HI}/M_\star \rangle$ (average)[b]	$M_{HI}/M_\star$ (median)[c]	N[d]
Log $M_\star$	10.16	0.272±0.034	0.262±0.035	0.117	105
	10.46	0.143±0.018	0.136±0.019	0.072	110
	10.77	0.084±0.009	0.078±0.009	0.044	116
	11.06	0.045±0.007	0.038±0.007	0.019	117
	11.30	0.028±0.005	0.019±0.006	0.017	32
Log $\mu_\star$	8.16	0.530±0.075	0.530±0.075	0.380	24
	8.46	0.296±0.045	0.291±0.046	0.191	50
	8.77	0.118±0.012	0.112±0.012	0.072	119
	9.07	0.069±0.006	0.060±0.006	0.034	193
	9.31	0.037±0.005	0.022±0.006	0.021	81
R_{90}/R_{50}	1.97	0.366±0.047	0.366±0.047	0.296	33
	2.35	0.279±0.039	0.276±0.039	0.143	91
	2.73	0.159±0.018	0.150±0.018	0.076	137
	3.10	0.062±0.007	0.049±0.007	0.026	176
	3.39	0.043±0.008	0.034±0.009	0.018	42
NUV−r	2.20	0.730±0.096	0.730±0.096	0.659	15
	2.85	0.366±0.040	0.366±0.040	0.233	65
	3.60	0.128±0.010	0.127±0.010	0.102	91
	4.36	0.106±0.012	0.103±0.012	0.069	79
	5.29	0.043±0.006	0.024±0.006	0.025	123
	5.83	0.027±0.004	0.011±0.004	0.017	94

Notes. — [a]Weighted, average gas fraction; HI mass of non-detections set to upper limit.
[b]Weighted, average gas fraction; HI mass of non-detections set to zero.
[c]Weighted, median gas fraction; HI mass of non-detections set to upper limit.
[d]Number of galaxies in the bin.

tected by ALFALFA or in the S05 archive that we did not re-observe with Arecibo, includes 480 galaxies, and marks the 50% of the full survey.

We discussed the properties of the 50% survey sample, and used it to revisit the scaling relations between gas mass fraction and galaxy structural parameters and color, as well as the gas fraction plane, presented in Paper 1. Overall our results confirm our previous findings, which were based on the initial 20% survey sample, and with almost identical scatters. However, the significantly improved statistics also allowed us to notice second-order effects, in the form of a systematic deviation of the high gas fraction tail in the $M_{HI}/M_\star$ versus NUV−r and gas fraction

plane relations. We identify the cause for such a deviation in the sensitivity limit of GASS, which is a gas fraction limited survey. Above a NUV$-r$ color of 4.5 mag, the results are dominated by the non-detections, which seem to cause an apparent break in the gas fraction versus color relation. As a result, the gas fraction plane slightly underpredicts $M_{\rm HI}/M_\star$ at the high end. Possible solutions include fitting the plane where the relation between gas fraction and NUV$-r$ is not dominated by the non-detections, or include additional parameters to the fit.

The new catalogs of HI, optical and UV parameters presented in this work increase the legacy value of GASS, and place our investigations of what physical processes are responsible for the transition between blue, star-forming galaxies and red, passively-evolving systems on a statistically more solid ground.

Acknowledgements. We thank the anonymous referee for useful suggestions.

This research has made use of the NASA/IPAC Extragalactic Database (NED) which is operated by the Jet Propulsion Laboratory, California Institute of Technology, under contract with the National Aeronautics and Space Administration.

The Arecibo Observatory is operated by SRI International under a cooperative agreement with the National Science Foundation (AST-1100968), and in alliance with Ana G. Méndez-Universidad Metropolitana, and the Universities Space Research Association.

GALEX (Galaxy Evolution Explorer) is a NASA Small Explorer, launched in April 2003. We gratefully acknowledge NASA's support for construction, operation, and science analysis for the GALEX mission, developed in cooperation with the Centre National d'Etudes Spatiales (CNES) of France and the Korean Ministry of Science and Technology.

Funding for the SDSS and SDSS-II has been provided by the Alfred P. Sloan Foundation, the Participating Institutions, the National Science Foundation, the U.S. Department of Energy, the National Aeronautics and Space Administration, the Japanese Monbukagakusho, the Max Planck Society, and the Higher Education Funding Council for England. The SDSS Web Site is http://www.sdss.org/.

The SDSS is managed by the Astrophysical Research Consortium for the Participating Institutions. The Participating Institutions are the American Museum of Natural History, Astrophysical Institute Potsdam, University of Basel, University of Cambridge, Case Western Reserve University, University of Chicago, Drexel University, Fermilab, the Institute for Advanced Study, the Japan Participation Group, Johns Hopkins University, the Joint Institute for Nuclear Astrophysics, the Kavli Institute for Particle Astrophysics and Cosmology, the Korean Scientist Group, the Chinese Academy of Sciences (LAMOST), Los Alamos National Laboratory, the Max-Planck-Institute for Astronomy (MPIA), the Max-Planck-Institute for Astrophysics (MPA), New Mexico State University, Ohio State University, University of Pittsburgh, University of Portsmouth, Princeton University, the United States Naval Observatory, and the University of Washington.

References

Adelman-McCarthy, J. K., Agüeros, M. A., Allam, S. S., et al. 2008, ApJS, 175, 297
Bernardi, M., Sheth, R. K., Annis, J., et al. 2003, AJ, 125, 1866
Binggeli, B., Sandage, A., & Tammann, G. A. 1985, AJ, 90, 1681
Boselli, A., Cortese, L., Deharveng, J. M., et al. 2005, ApJ, 629, L29
Boselli, A., Eales, S., Cortese, L., et al. 2010, PASP, 122, 261
Catinella, B., Kauffmann, G., Schiminovich, D., et al. 2012, MNRAS, 420, 1959
Catinella, B., Schiminovich, D., Kauffmann, G., et al. 2010, MNRAS, 403, 683 (Paper 1)
Chabrier, G. 2003, PASP, 115, 763
Cortese, L., Catinella, B., Boissier, S., Boselli, A., & Heinis, S. 2011, MNRAS, 415, 1797
Cortese, L. & Hughes, T. M. 2009, MNRAS, 400, 1225
Courtois, H. M., Tully, R. B., Fisher, J. R., et al. 2009, AJ, 138, 1938
Davé, R., Finlator, K., & Oppenheimer, B. D. 2011, MNRAS, 416, 1354
Dreyer, J. L. E. 1888, MmRAS, 49, 1
Dreyer, J. L. E. 1895, MmRAS, 51, 185
Dreyer, J. L. E. 1908, MmRAS, 59, 105
Fabello, S., Catinella, B., Giovanelli, R., et al. 2011, MNRAS, 411, 993
Fu, J., Guo, Q., Kauffmann, G., & Krumholz, M. R. 2010, MNRAS, 409, 515
Giovanelli, R., Haynes, M. P., Kent, B. R., et al. 2005, AJ, 130, 2598
Haynes, M. P., Giovanelli, R., Martin, A. M., et al. 2011, AJ, 142, 170
Kauffmann, G., Li, C., Fu, J., et al. 2012, MNRAS, 422, 997
Kennicutt, Jr., R. C. 1998, ApJ, 498, 541
Lagos, C. D. P., Baugh, C. M., Lacey, C. G., et al. 2011, MNRAS, 418, 1649
Li, C., Kauffmann, G., Fu, J., et al. 2012, MNRAS, in press (arXiv:1202.2857)
Martin, D. C., Fanson, J., Schiminovich, D., et al. 2005, ApJ, 619, L1
Moran, S. M., Heckman, T. M., Kauffmann, G., et al. 2012, ApJ, 745, 66
Moran, S. M., Kauffmann, G., Heckman, T. M., et al. 2010, ApJ, 720, 1126
Nilson, P. 1973, Uppsala general catalogue of galaxies (Uppsala: Astron. Obs. Pub.) (UGC)
O'Connell, R. W. 1999, ARA&A, 37, 603
Roberts, M. S. & Haynes, M. P. 1994, ARA&A, 32, 115
Saintonge, A. 2007, AJ, 133, 2087
Saintonge, A., Kauffmann, G., Kramer, C., et al. 2011a, MNRAS, 415, 32
Saintonge, A., Kauffmann, G., Wang, J., et al. 2011b, MNRAS, 415, 61
Salim, S., Rich, R. M., Charlot, S., et al. 2007, ApJS, 173, 267
Sancisi, R., Fraternali, F., Oosterloo, T., & van der Hulst, T. 2008, A&A Rev., 15, 189
Schiminovich, D., Catinella, B., Kauffmann, G., et al. 2010, MNRAS, 408, 919
Schmidt, M. 1963, ApJ, 137, 758
Schneider, S. E., Thuan, T. X., Magri, C., & Wadiak, J. E. 1990, ApJS, 72, 245
Springob, C. M., Haynes, M. P., Giovanelli, R., & Kent, B. R. 2005, ApJS, 160, 149 (S05)
Walter, F., Brinks, E., de Blok, W. J. G., et al. 2008, AJ, 136, 2563
Wang, J., Kauffmann, G., Overzier, R., et al. 2011, MNRAS, 412, 1081
Wang, J., Overzier, R., Kauffmann, G., von der Linden, A., & Kong, X. 2010, MNRAS, 401, 433
Wyder, T. K., Martin, D. C., Schiminovich, D., et al. 2007, ApJS, 173, 293
York, D. G., Adelman, J., Anderson, Jr., J. E., et al. 2000, AJ, 120, 1579
Zhang, W., Li, C., Kauffmann, G., et al. 2009, MNRAS, 397, 1243
Zwicky, F., Herzog, E., Wild, P., Karpowicz, M., & Kowal, C. T. 1961-1968, Catalogue of galaxies and of clusters of galaxies (Pasadena: Caltech) (CGCG)

Appendix A: GASS DR2 spectra and tables

We present here SDSS postage stamp images, Arecibo HI-line spectra, and catalogs of optical, UV and HI parameters for the 240 galaxies included in this second data release. The figures are organized as follows:

- Figure A.1: HI detections.
- Figure A.2: marginal HI detections (cataloged as "quality code 2" in Table A.2.
- Figure A.3: marginal HI detections that are also confused within the Arecibo beam (cataloged as "quality code 3" in Table A.2.
- Figure A.4: HI detections that are confused within the Arecibo beam (cataloged as "quality code 5" in Table A.2.
- Figure A.5: HI non-detections.

The tables include SDSS and UV parameters for the 240 galaxies (Table A.1), HI measurements for the 133 detections (Table A.2), and HI upper limits for the 107 non-detections (Table A.3). For the detailed content of the tables, see Section 3. Notes on individual objects (marked with an asterisk in the last column of Tables A.2 and A.3) are reported in Appendix B.

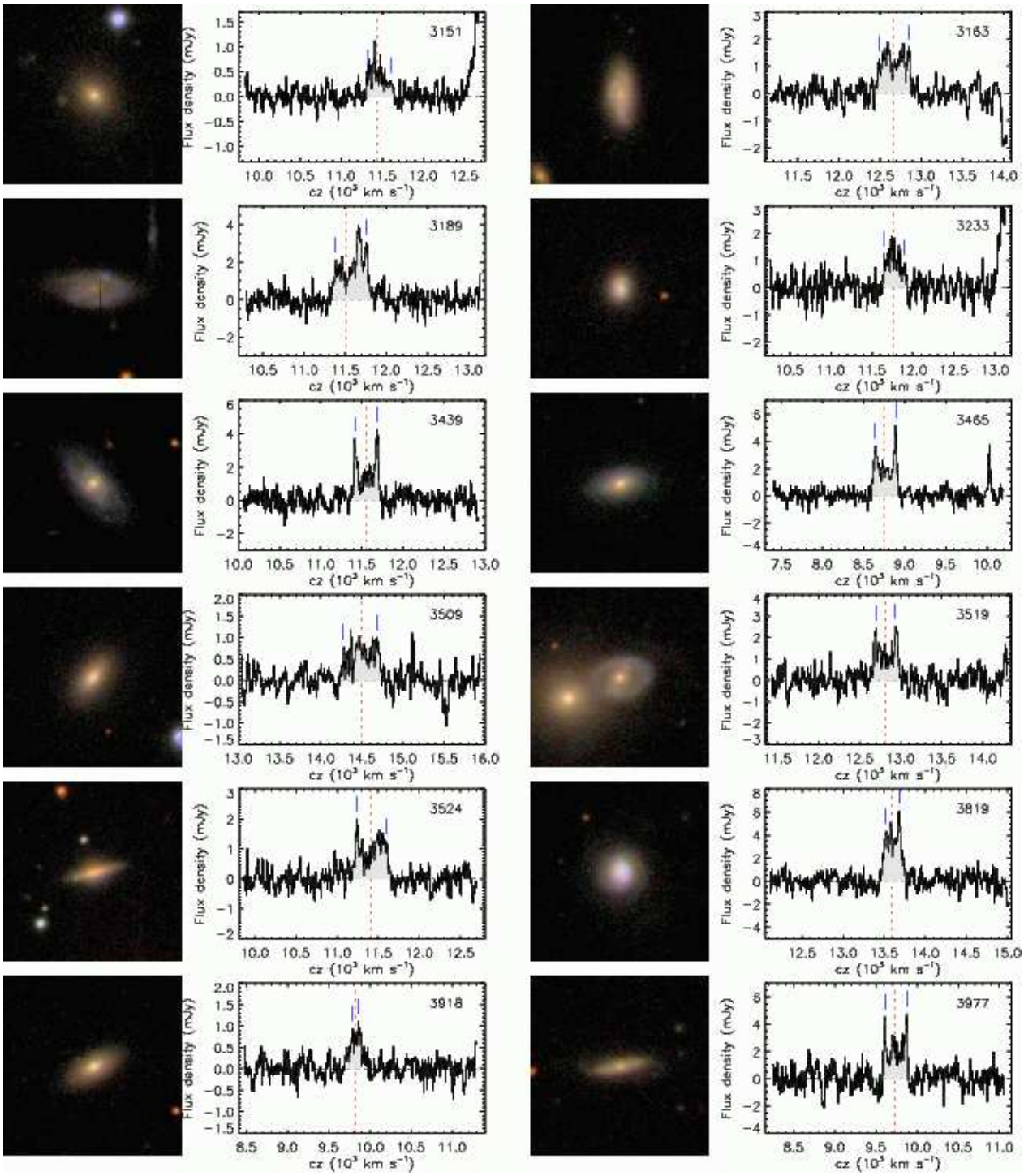

Fig. A.1. SDSS postage stamp images (1 arcmin square) and HI-line profiles of the detections included in this second data release, ordered by increasing GASS number (indicated in each spectrum). The HI spectra are calibrated, smoothed and baseline-subtracted. A dotted line and two dashes indicate the heliocentric velocity corresponding to the SDSS redshift and the two peaks used for width measurement, respectively. *Only the first page is shown here.*

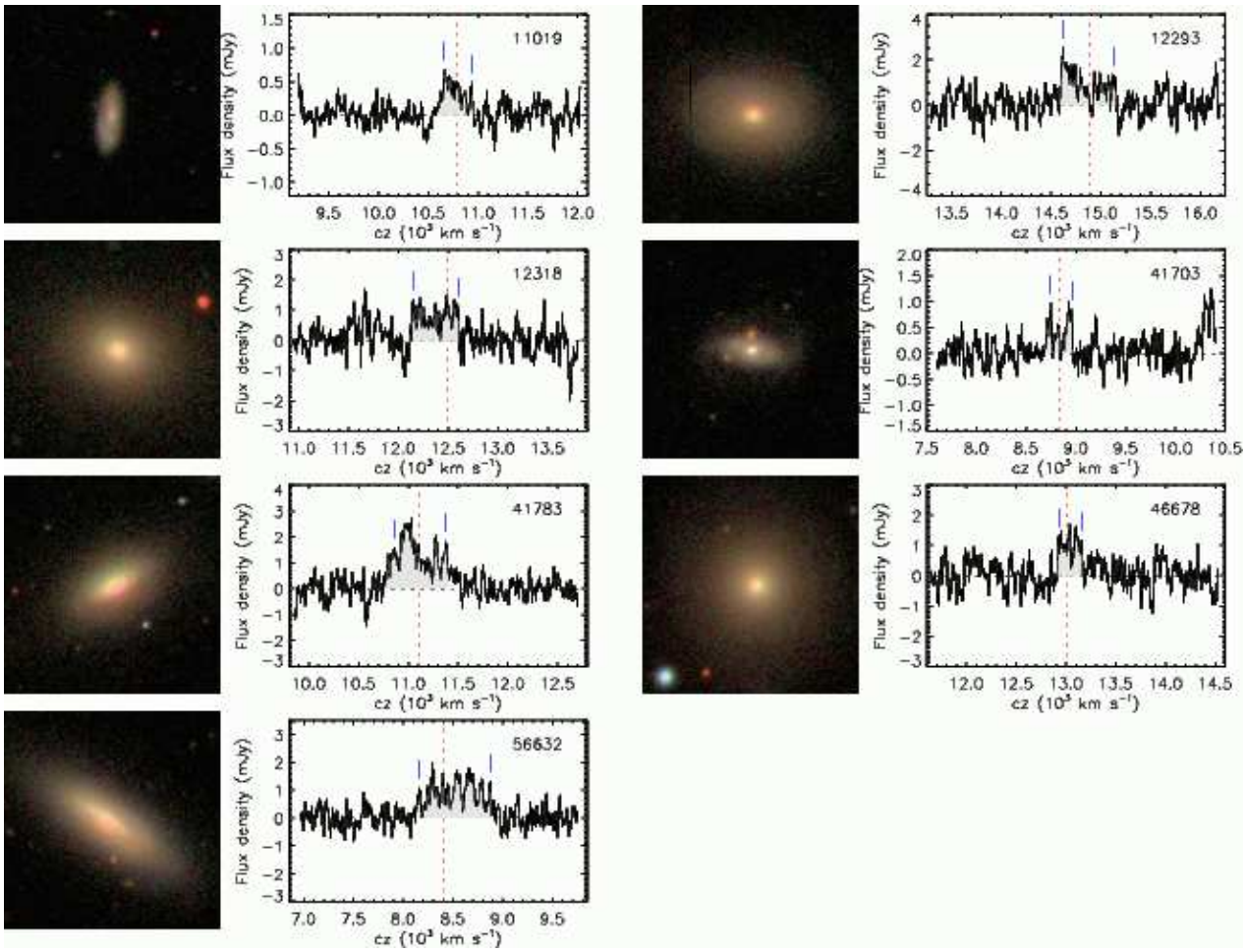

Fig. A.2. Same as Figure A.1 for marginal detections (code 2).

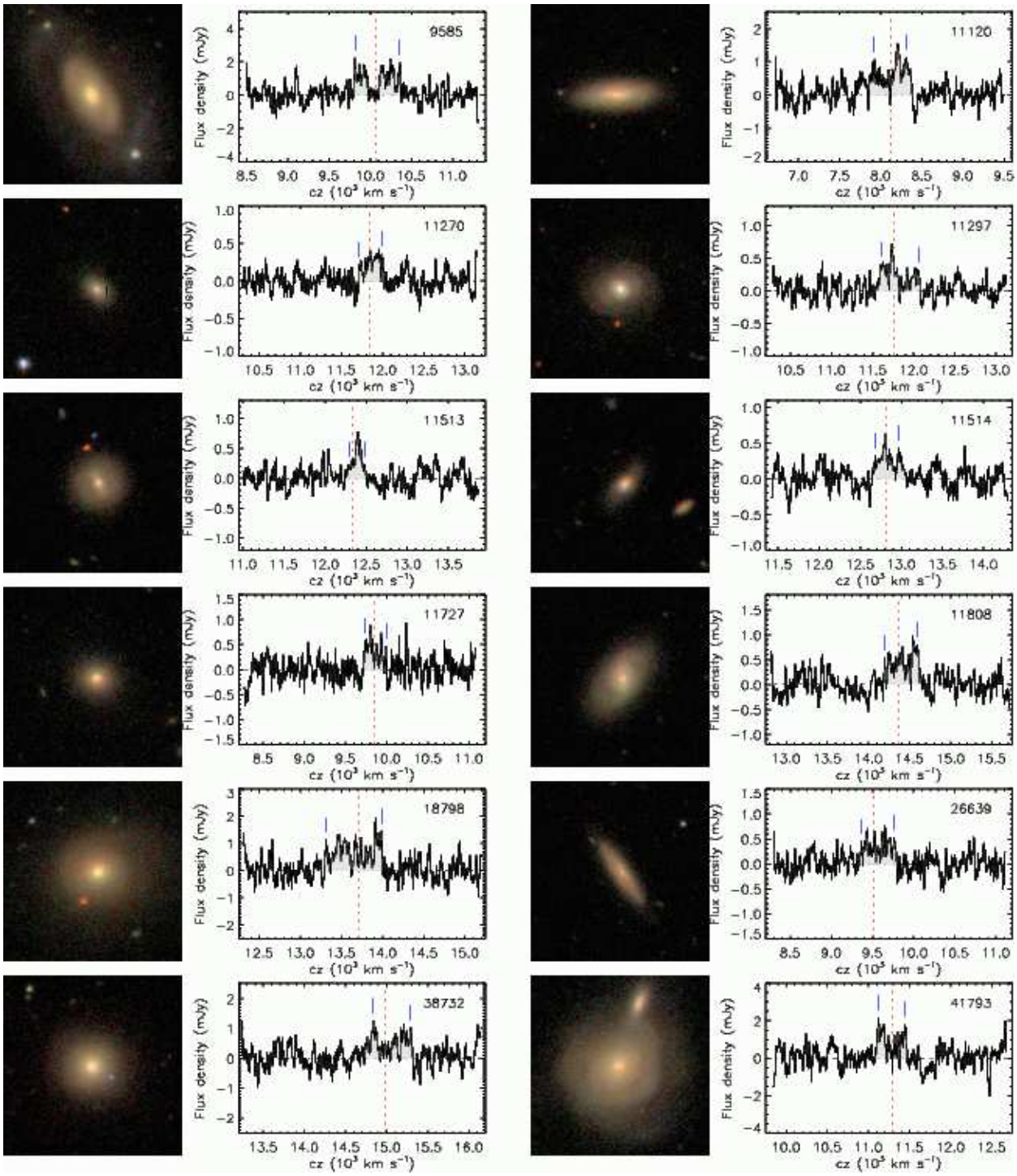

Fig. A.3. Same as Figure A.1 for marginal detections (code 3).

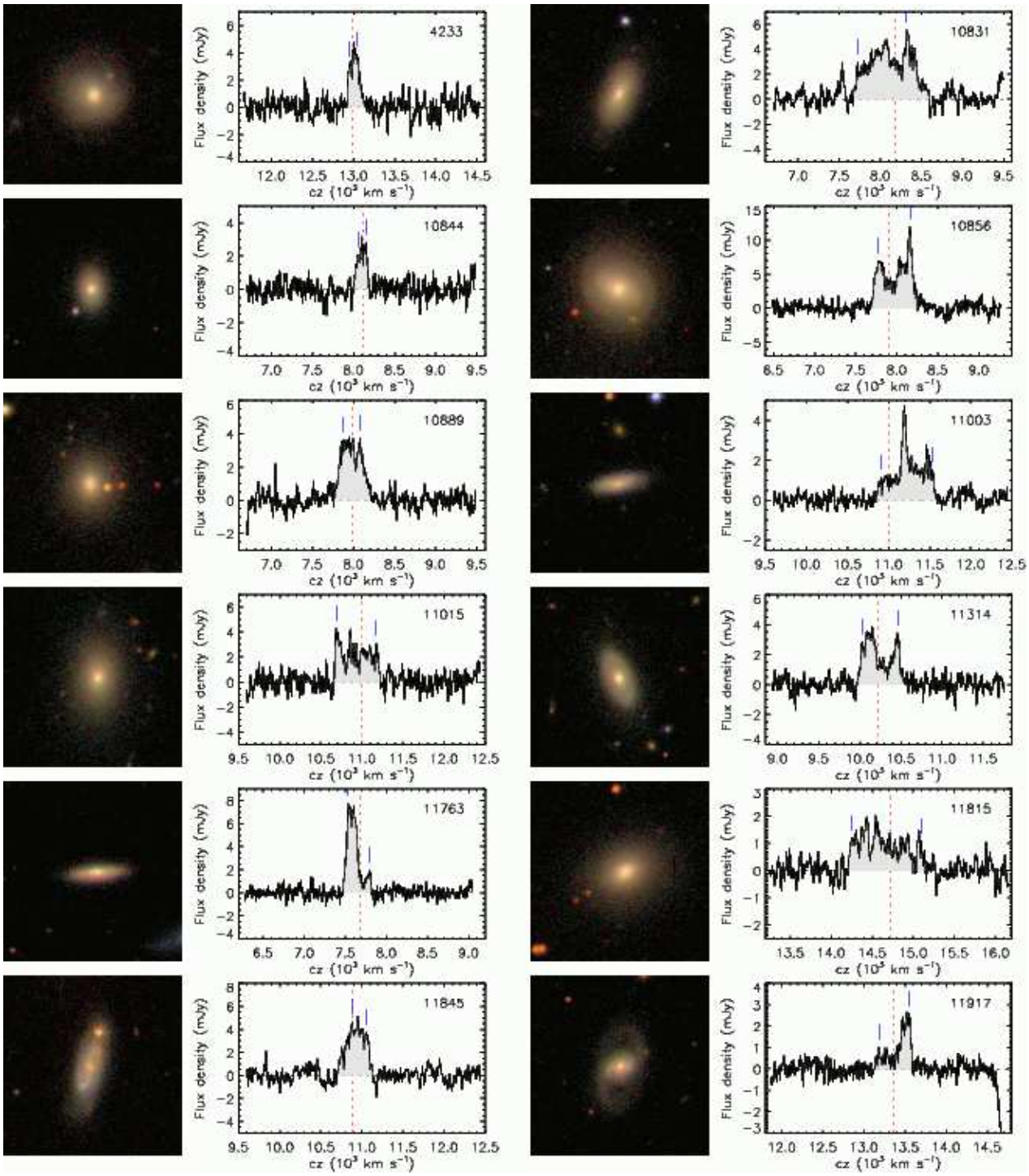

Fig. A.4. Same as Figure A.1 for confused detections (code 5). *Only the first page is shown here.*

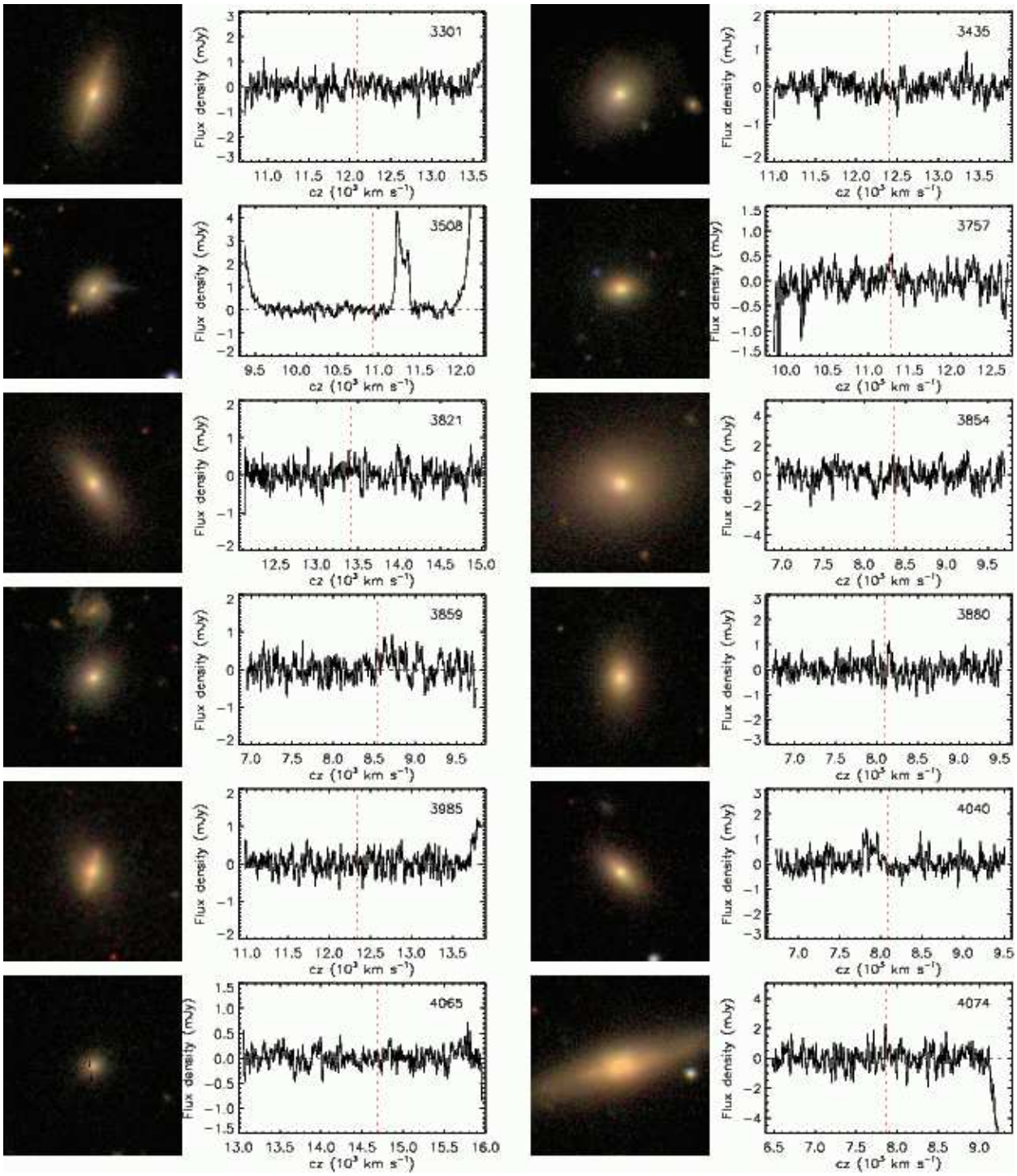

Fig. A.5. Same as Figure A.1 for non-detections. *Only the first page is shown here.*

Table A.1. SDSS and UV Parameters of the GASS Galaxies.

GASS (1)	SDSS ID (2)	Other name (3)	$z_{\rm SDSS}$ (4)	Log $M_\star$ ($M_\odot$) (5)	$R_{50,z}$ ($''$) (6)	R_{50} ($''$) (7)	R_{90} ($''$) (8)	Log $\mu_\star$ ($M_\odot$ kpc^{-2}) (9)	ext$_r$ (mag) (10)	r (mag) (11)	(b/a)$_r$ (12)	incl (deg) (13)	NUV$-r$ (mag) (14)	T$_{NUV}$ (sec) (15)	$T_{\rm max}$ (min) (16)
11834	J000047.89+141639.1	...	0.0362	10.71	3.21	3.55	10.51	9.12	0.17	15.15	0.341	74	3.94	1671	24
11825	J000210.19+140810.3	...	0.0420	10.62	2.17	2.16	7.01	9.25	0.19	15.45	0.719	45	5.68	364	65
11917	J000742.65+151112.7	...	0.0446	10.74	2.96	3.39	10.45	9.04	0.18	15.25	0.677	49	4.06	1680	48
12005	J002420.72+144632.3	...	0.0309	10.06	1.71	1.79	5.09	9.16	0.17	16.04	0.348	73	5.05	3519	33
12002	J002504.00+145815.2	...	0.0367	10.48	1.75	1.81	5.74	9.41	0.14	15.47	0.424	68	6.25	3519	66
3163	J002846.83+150529.3	...	0.0422	10.63	3.99	4.23	9.19	8.72	0.17	15.12	0.468	64	3.82	3133	64
3151	J003143.05+142911.2	...	0.0381	10.40	2.90	3.40	11.16	8.85	0.19	15.51	0.784	39	4.85	3133	77
27181	J003248.17+144738.1	...	0.0418	10.60	3.38	3.67	10.23	8.84	0.18	15.11	0.781	40	3.22	1659	73
27167	J003921.66+142811.5	...	0.0380	10.37	2.02	2.15	5.96	9.14	0.27	15.49	0.711	46	4.48	1658	76
3189	J004023.48+143649.4	...	0.0384	10.05	5.59	5.96	11.68	7.92	0.32	15.66	0.471	64	2.77	1658	80
27219	J004125.29+134334.3	...	0.0332	10.21	4.34	4.33	9.51	8.44	0.23	16.43	0.253	81	3.96	1658	44
3233	J005134.04+135452.7	...	0.0392	10.23	2.31	2.35	5.82	8.85	0.20	15.67	0.708	46	3.28	175	87
3301	J005915.31+133433.3	...	0.0404	10.92	3.55	3.65	11.61	9.15	0.19	14.55	0.491	63	6.13	3142	14
3435	J010832.07+150122.9	...	0.0414	10.76	3.29	3.54	11.80	9.03	0.17	14.61	0.769	41	5.40	1648	33
3439	J010905.96+144520.8	...	0.0386	10.35	2.96	3.56	10.34	8.78	0.14	15.48	0.790	39	3.05	1648	81
3465	J011221.82+150039.0	...	0.0292	10.19	2.75	3.07	8.87	8.93	0.13	15.33	0.570	57	3.63	1648	26
3509	J011711.65+132027.3	...	0.0484	10.81	2.50	2.68	8.33	9.18	0.09	15.28	0.562	58	4.14	1647	51
3524	J011716.09+143720.5	...	0.0380	10.73	2.38	2.66	7.22	9.36	0.10	15.58	0.337	74	5.15	1608	27
3519	J011728.11+144215.9	UGC827	0.0427	10.74	4.93	5.31	11.67	8.64	0.11	14.95	0.736	44	3.68	1647	40
3508	J011900.04+143643.1	...	0.0365	10.37	2.90	2.98	7.45	8.87	0.10	15.55	0.723	45	5.12	6090	64
3757	J012227.97+153238.4	...	0.0376	10.52	1.93	2.14	6.43	9.34	0.31	15.25	0.665	50	4.92	1658	65
3854	J013854.76+150117.7	CGCG437-008	0.0279	10.91	5.67	6.35	20.16	9.06	0.16	13.76	0.785	39	5.58	2954	3
3859	J013901.89+145808.5	...	0.0285	10.18	2.92	3.26	10.53	8.88	0.15	15.38	0.780	40	4.96	2954	23
3821	J014042.68+133304.6	...	0.0447	10.87	3.21	3.26	10.63	9.09	0.15	14.85	0.561	58	5.84	1604	27
3819	J014143.18+134032.8	...	0.0453	10.67	2.63	2.74	6.81	9.06	0.15	14.72	0.871	30	2.20	3361	72
4094	J014326.66+131913.0	...	0.0276	10.55	3.15	3.18	9.47	9.22	0.13	14.71	0.581	56	5.94	1696	16
4119	J014629.79+135709.6	...	0.0444	11.19	4.26	4.85	15.59	9.18	0.14	14.22	0.776	40	6.13	1625	6
4195	J014906.09+142550.6	...	0.0445	10.62	3.96	4.57	13.20	8.66	0.14	15.31	0.686	48	4.74	1677	85
4074	J014911.62+125111.6	UGC1274	0.0262	11.17	3.86	4.16	12.80	9.71	0.22	13.41	0.489	63	6.03	1644	1
4065	J014941.82+124458.2	...	0.0490	10.17	2.40	2.53	7.66	8.56	0.21	16.57	0.917	24	5.31	1644	217
4203	J015027.35+141140.0	...	0.0341	10.18	4.65	4.67	10.29	8.33	0.14	15.70	0.373	71	3.45	1661	49
4145	J015517.63+125935.5	...	0.0322	10.30	2.18	2.43	7.68	9.16	0.15	15.09	0.419	68	3.04	1659	39
4137	J015651.99+131246.0	...	0.0445	10.90	2.59	2.78	9.25	9.32	0.14	15.00	0.573	57	5.35	1651	23
4233	J015707.32+145543.5	...	0.0433	10.88	3.59	3.94	12.05	9.03	0.16	14.70	0.883	29	5.69	1671	23
4223	J015712.97+144407.6	CGCG438-008	0.0260	10.56	3.62	3.96	13.26	9.16	0.14	14.44	0.971	14	5.19	1671	12
3918	J015718.40+130745.8	...	0.0327	10.38	2.12	2.11	6.72	9.24	0.15	15.30	0.556	58	5.69	1651	41
4017	J020517.54+133020.6	IC1775	0.0258	10.23	6.78	10.39	19.52	8.29	0.24	14.44	0.908	25	3.17	1662	16
3880	J020519.88+131530.7	...	0.0270	10.52	2.77	2.80	8.35	9.33	0.28	14.61	0.714	46	6.00	1662	17
3977	J020744.46+140453.7	...	0.0324	10.26	3.76	4.28	11.18	8.64	0.22	15.60	0.270	79	3.57	1645	40
4030	J020939.47+135859.4	...	0.0491	11.33	7.64	8.32	16.80	8.72	0.26	14.08	0.822	36	4.08	1531	5
4038	J021121.82+143015.5	UGC1681	0.0417	10.72	4.83	5.95	15.25	8.65	0.28	15.10	0.223	84	3.40	1531	41
4039	J021131.43+141202.4	...	0.0254	10.32	3.69	4.33	12.75	8.93	0.25	14.80	0.675	49	3.47	1531	15
4040	J021139.06+140830.3	...	0.0269	10.32	2.32	2.36	7.43	9.27	0.25	14.99	0.530	60	5.80	1531	19
4048	J021219.38+133645.6	...	0.0414	10.55	3.51	3.75	8.71	8.77	0.30	15.40	0.615	54	3.45	1692	84
3981	J021404.39+131156.3	...	0.0416	10.55	3.51	3.81	9.96	8.76	0.34	15.34	0.497	62	3.76	1692	88
3985	J021412.12+132612.8	...	0.0411	10.76	3.48	3.73	10.56	8.98	0.33	15.09	0.617	53	5.95	1692	33
4057	J021419.24+135611.2	...	0.0397	10.52	2.34	2.64	7.19	9.13	0.34	15.27	0.505	62	3.36	1654	81

Table A.1. continued.

GASS (1)	SDSS ID (2)	Other name (3)	z_{SDSS} (4)	Log $M_\star$ ($M_\odot$) (5)	$R_{50,z}$ ($''$) (6)	R_{50} ($''$) (7)	R_{90} ($''$) (8)	Log $\mu_\star$ ($M_\odot$ kpc^{-2}) (9)	ext$_r$ (mag) (10)	r (mag) (11)	(b/a)$_r$ (12)	incl (deg) (13)	NUV−r (mag) (14)	T$_{NUV}$ (sec) (15)	$T_{\max}$ (min) (16)
51416	J075559.95+125853.2	CGCG058-073	0.0445	11.27	3.98	4.54	14.53	9.31	0.09	13.92	0.860	31	5.43	208	4
56319	J080322.76+095745.8	...	0.0345	10.14	3.39	3.28	8.31	8.54	0.07	16.70	0.272	79	4.78	223	51
56304	J080534.10+102336.2	UGC4215	0.0340	10.89	7.43	15.04	26.90	8.63	0.06	14.18	0.812	37	3.61	218	8
56632	J090437.07+133314.7	CGCG061-057	0.0281	11.00	4.92	5.35	15.02	9.27	0.10	13.59	0.372	71	4.94	1612	2
16753	J091828.43+062003.7	...	0.0335	10.29	3.57	3.93	11.23	8.68	0.12	15.21	0.623	53	3.41	1706	45
25844	J091959.74+100631.7	...	0.0326	10.25	1.43	1.47	4.05	9.46	0.13	15.65	0.503	62	5.62	1677	41
8347	J093858.50+040940.5	...	0.0463	10.68	2.65	2.71	7.72	9.04	0.12	15.29	0.863	31	6.04	2114	76
18702	J095051.58+081340.7	...	0.0299	10.20	3.50	3.86	8.49	8.71	0.10	15.71	0.255	81	3.84	1676	28
18707	J095150.14+082213.8	...	0.0405	10.57	3.04	3.33	8.61	8.93	0.13	14.95	0.596	55	3.33	207	71
20305	J095243.86+100001.0	...	0.0303	10.30	4.92	5.47	12.13	8.50	0.10	15.68	0.190	90	4.75	112	30
18673	J095301.79+072736.4	...	0.0385	10.38	2.47	2.67	6.07	8.97	0.12	15.32	0.659	50	3.04	1249	81
18686	J095302.62+075029.3	CGCG035-075	0.0411	10.55	4.91	5.76	12.10	8.48	0.11	14.89	0.606	54	2.99	1676	83
18681	J095324.56+074956.2	...	0.0393	10.67	3.66	3.95	11.00	8.90	0.11	15.40	0.260	80	4.22	1676	39
20292	J095349.23+091137.6	CGCG063-098	0.0299	10.67	4.22	4.53	10.91	9.02	0.13	14.38	0.776	40	4.47	3178	13
20371	J095402.22+103629.6	CGCG063-101	0.0399	11.24	6.35	7.62	21.70	8.97	0.08	13.84	0.764	41	5.38	208	3
20448	J095812.59+110635.5	...	0.0272	10.06	2.04	2.17	6.07	9.12	0.08	15.40	0.587	56	3.26	109	20
18755	J100057.16+073743.2	CGCG036-018	0.0489	11.31	5.81	6.54	19.49	8.94	0.07	14.10	0.829	35	5.80	224	5
14863	J100134.25+065555.3	CGCG036-021	0.0489	11.39	4.83	5.33	16.05	9.17	0.06	14.15	0.567	57	5.95	330	4
5035	J100152.69+030040.7	...	0.0441	10.77	2.91	3.09	9.94	9.10	0.07	14.82	0.661	50	3.72	10840	40
18830	J101100.68+085920.7	...	0.0320	10.27	2.41	2.56	8.01	9.05	0.08	15.34	0.702	47	4.67	320	38
18798	J101329.66+075415.5	CGCG036-062	0.0458	11.22	4.58	5.35	17.20	9.11	0.09	14.24	0.776	40	5.12	419	6
18875	J102004.22+074622.1	CGCG037-002	0.0451	11.11	4.62	4.85	16.29	9.01	0.07	14.34	0.673	49	5.47	6825	9
18877	J102025.15+074037.8	CGCG037-003	0.0452	10.97	4.37	4.64	11.75	8.91	0.07	14.62	0.435	67	4.08	336	18
18872	J102039.65+075133.9	CGCG037-006	0.0451	11.13	4.25	4.48	15.17	9.11	0.07	14.26	0.679	49	5.93	6825	8
18887	J102055.54+081849.4	...	0.0458	10.76	3.38	3.66	10.62	8.92	0.08	15.42	0.333	74	3.95	6825	49
54233	J102157.80+243918.7	IC2567	0.0402	11.14	5.95	7.00	17.63	8.92	0.06	14.03	0.479	64	5.19	112	5
26320	J102238.71+120517.8	...	0.0450	10.71	2.35	2.43	7.15	9.20	0.11	15.48	0.624	53	4.89	112	59
18862	J102241.20+082003.2	...	0.0446	10.68	4.00	4.28	11.77	8.71	0.09	15.19	0.544	59	3.81	254	66
26336	J102316.17+130528.7	CGCG065-013	0.0320	11.00	4.91	5.18	15.76	9.16	0.13	14.00	0.634	52	6.06	322	4
26319	J102339.36+130227.4	...	0.0322	10.29	2.84	3.02	8.45	8.91	0.12	15.44	0.476	64	5.26	322	39
23026	J102721.97+110447.9	UGC5665	0.0323	11.16	6.25	7.50	23.74	9.10	0.09	13.94	0.374	71	5.29	335	2
23069	J102742.61+104927.6	...	0.0316	10.22	3.36	3.51	10.11	8.71	0.09	15.51	0.826	35	5.60	335	36
23039	J102756.01+111444.6	...	0.0325	10.78	3.04	3.22	10.29	9.34	0.09	14.24	0.671	49	5.68	335	11
54763	J103721.85+272131.4	CGCG154-033	0.0421	11.11	6.00	5.10	19.39	8.84	0.06	14.38	0.821	36	4.83	192	7
26570	J103905.90+132153.5	...	0.0325	10.00	4.02	4.21	9.15	8.32	0.12	15.66	0.865	31	2.97	326	40
23227	J103913.15+121130.9	...	0.0479	11.18	4.30	4.64	14.77	9.09	0.07	14.51	0.372	71	4.85	1565	9
23228	J103920.02+114128.1	...	0.0479	11.04	3.02	3.18	10.10	9.26	0.09	14.70	0.880	29	5.62	219	16
15211	J104024.66+065137.7	...	0.0303	10.89	4.48	5.79	17.15	9.17	0.10	14.70	0.343	73	4.64	695	5
26640	J104028.50+133721.9	CGCG065-082	0.0317	10.99	5.88	6.59	20.47	9.00	0.10	13.81	0.745	43	5.97	326	4
26639	J104046.05+134659.9	...	0.0317	10.24	4.21	4.33	10.59	8.54	0.10	15.88	0.287	78	5.42	326	36
15166	J104121.14+061644.3	CGCG037-116	0.0339	10.02	5.00	5.62	11.62	8.10	0.07	15.33	0.427	67	2.35	2583	48
29555	J104145.56+135352.9	...	0.0316	10.38	3.33	3.63	11.29	8.88	0.09	14.94	0.767	41	4.55	326	36
57099	J104221.91+152134.6	IC637	0.0490	11.10	5.12	5.83	17.88	8.84	0.09	14.05	0.839	34	4.71	200	13
15151	J104251.39+055135.5	CGCG037-125	0.0334	10.99	4.21	4.60	13.51	9.24	0.06	14.39	0.378	71	4.93	2583	5
29594	J104639.64+140647.4	...	0.0336	10.03	3.06	3.08	8.95	8.56	0.09	16.01	0.350	73	5.33	1831	46
15242	J105016.92+060721.3	CGCG038-026	0.0422	10.61	2.81	2.77	8.99	9.00	0.08	14.96	0.658	50	5.60	1573	72
23437	J105147.93+115901.7	...	0.0465	10.91	3.54	3.74	11.98	9.01	0.05	14.78	0.675	49	5.35	427	27

Table A.1. continued.

GASS (1)	SDSS ID (2)	Other name (3)	z_{SDSS} (4)	Log $M_\star$ ($M_\odot$) (5)	$R_{50,z}$ ($''$) (6)	R_{50} ($''$) (7)	R_{90} ($''$) (8)	Log $\mu_\star$ ($M_\odot$ kpc^{-2}) (9)	ext$_r$ (mag) (10)	r (mag) (11)	(b/a)$_r$ (12)	incl (deg) (13)	NUV$-r$ (mag) (14)	T$_{NUV}$ (sec) (15)	$T_{\max}$ (min) (16)
54986	J105739.31+272937.1	...	0.0454	11.19	5.51	5.89	16.43	8.93	0.06	14.16	0.966	15	5.79	192	7
17684	J110037.27+102613.9	IC663	0.0361	11.08	5.44	5.68	14.05	9.04	0.08	14.13	0.714	46	6.05	329	4
29624	J110050.33+133551.4	...	0.0340	10.32	4.02	5.12	12.76	8.59	0.04	15.92	0.250	81	4.17	1642	48
23518	J110103.65+120827.7	...	0.0342	10.43	3.10	3.10	8.87	8.92	0.05	15.30	0.409	69	7.14	107	50
23563	J110741.70+130132.4	CGCG066-117	0.0350	11.26	6.66	6.91	19.94	9.07	0.04	13.45	0.636	52	5.62	205	2
47896	J110851.20+282832.5	UGC6191	0.0363	11.12	6.30	7.56	18.44	8.95	0.07	13.76	0.786	39	3.73	199	4
17840	J111254.48+093050.3	...	0.0291	10.19	2.03	2.15	6.37	9.20	0.07	15.29	0.555	58	5.05	1605	25
15612	J111341.33+074545.9	MRK1295	0.0291	10.53	2.15	2.14	6.54	9.49	0.09	14.84	0.706	46	5.87	1607	22
12318	J111443.35+040128.2	CGCG039-088	0.0417	11.21	4.36	4.64	15.23	9.23	0.13	13.88	0.774	40	5.60	2466	4
23539	J111447.94+114735.0	...	0.0379	10.19	1.74	1.76	4.76	9.10	0.05	15.99	0.466	65	5.76	1612	76
12293	J112029.23+040742.1	CGCG039-127	0.0496	11.32	6.20	7.32	17.61	8.87	0.12	14.16	0.706	46	4.44	1536	5
29892	J112946.35+152001.1	CGCG096-056	0.0366	11.02	4.86	5.51	15.68	9.06	0.10	13.88	0.576	57	3.81	119	6
23757	J113645.51+132009.9	...	0.0342	10.51	3.26	3.55	9.70	8.96	0.10	14.83	0.458	65	3.63	341	47
12597	J114309.53+055557.8	...	0.0315	10.31	2.31	2.19	6.62	9.13	0.07	15.40	0.455	65	5.45	2614	35
18087	J114940.66+094255.1	...	0.0352	10.39	2.57	2.77	7.85	9.02	0.07	15.32	0.861	31	4.55	90	56
18202	J121134.94+092106.8	...	0.0269	10.25	2.86	2.94	8.64	9.02	0.05	15.00	0.889	28	5.55	76	19
30192	J121418.23+142345.8	...	0.0251	10.43	2.81	2.80	9.49	9.29	0.11	14.66	0.568	57	5.18	109	14
24168	J121612.36+132615.4	...	0.0260	10.44	4.49	4.92	13.94	8.85	0.09	14.96	0.280	78	4.77	2601	16
28057	J122532.62+080301.4	...	0.0381	10.30	6.31	6.71	12.34	8.08	0.06	15.37	0.768	41	2.95	3272	77
18482	J123053.16+090456.9	...	0.0393	10.43	1.93	1.97	6.42	9.21	0.05	15.61	0.735	44	5.54	311	88
12970	J123553.79+054539.8	VCC1643	0.0418	10.89	6.94	7.83	21.60	8.51	0.07	14.39	0.782	40	5.50	3047	18
18576	J123625.93+085639.7	...	0.0277	10.26	3.36	3.61	9.50	8.87	0.06	15.10	0.606	54	4.13	1696	21
24366	J123938.86+122507.9	...	0.0411	10.86	2.16	2.23	7.23	9.51	0.13	14.96	0.420	68	5.76	3791	20
24437	J123949.27+133256.8	CGCG070-205	0.0466	10.67	2.72	2.90	8.02	9.00	0.09	15.60	0.471	64	3.74	189	81
28482	J124307.28+111243.1	IC3694	0.0282	10.23	5.38	5.45	12.53	8.42	0.08	14.63	0.694	47	2.32	1658	23
28462	J124618.26+115224.8	IC3760	0.0449	10.73	2.55	2.67	7.77	9.16	0.07	15.11	0.581	56	5.62	2285	51
28461	J124622.67+115235.7	IC815	0.0443	11.36	5.08	5.33	17.71	9.19	0.07	13.76	0.834	34	5.87	2285	3
13091	J125451.85+035305.4	CGCG043-063	0.0483	11.44	5.16	5.45	18.02	9.18	0.10	13.77	0.726	45	5.71	305	3
28551	J125657.07+122148.6	...	0.0496	11.18	3.39	3.74	12.12	9.26	0.09	14.67	0.412	68	5.68	259	10
25167	J130256.89+125250.0	...	0.0362	10.49	3.58	4.15	12.15	8.81	0.07	15.05	0.367	72	4.16	109	62
40425	J130404.23+084820.6	...	0.0358	10.17	4.02	4.40	10.77	8.40	0.09	15.65	0.326	75	2.97	253	59
13158	J130454.21+034928.1	UGC8173	0.0410	10.81	4.52	5.23	13.28	8.81	0.08	14.35	0.807	37	2.61	3371	25
6749	J130750.80+031140.7	UGC8208	0.0386	11.12	6.08	7.17	18.45	8.92	0.07	14.06	0.266	80	4.25	121	5
25236	J131357.26+123533.2	CGCG072-031	0.0256	10.24	4.09	4.20	12.53	8.76	0.06	14.75	0.908	25	5.16	103	15
25202	J131415.99+120348.5	...	0.0343	10.52	3.04	3.20	8.39	9.03	0.07	14.64	0.680	48	5.29	111	45
26911	J131621.43+133006.6	CGCG072-041	0.0304	10.98	5.13	5.56	18.21	9.14	0.06	13.71	0.829	35	...	...	3
25296	J132357.45+120233.3	CGCG072-063	0.0390	11.01	2.80	3.24	9.55	9.47	0.08	14.44	0.580	56	4.13	96	8
34531	J132939.26+294612.3	UGC8483	0.0472	11.27	5.71	6.72	21.22	8.94	0.03	14.04	0.779	40	5.63	144	5
51190	J134404.06+253948.6	...	0.0486	11.03	4.98	5.66	13.16	8.79	0.04	14.42	0.445	66	3.70	367	19
13551	J134505.90+034815.3	...	0.0331	10.05	2.77	2.91	7.86	8.67	0.06	15.75	0.553	58	4.81	2971	44
25475	J134807.60+112405.1	...	0.0360	10.34	2.18	2.43	6.73	9.09	0.09	15.58	0.619	53	...	...	61
13624	J135152.41+032718.0	CGCG045-119	0.0296	10.31	5.86	6.45	13.70	8.38	0.09	14.41	0.670	49	2.50	1626	28
44846	J135512.58+250117.1	IC4344	0.0310	11.00	6.90	8.01	21.60	8.89	0.04	13.65	0.687	48	4.61	268	3
40260	J135827.10+132904.7	CGCG074-022	0.0388	10.77	3.10	3.18	10.03	9.15	0.07	14.89	0.571	57	5.29	240	24
25572	J140700.00+130019.1	CGCG074-109	0.0274	10.45	3.20	3.52	12.21	9.12	0.07	14.74	0.446	66	5.22	110	20
41303	J140741.05+094835.8	...	0.0374	10.23	2.02	1.99	5.80	9.01	0.07	15.95	0.584	56	6.60	109	72
38538	J141119.35+113105.1	...	0.0385	10.13	2.73	2.94	8.81	8.63	0.06	15.74	0.885	28	3.38	106	80

Table A.1. continued.

GASS (1)	SDSS ID (2)	Other name (3)	z_{SDSS} (4)	Log $M_\star$ ($M_\odot$) (5)	$R_{50,z}$ ($''$) (6)	R_{50} ($''$) (7)	R_{90} ($''$) (8)	Log $\mu_\star$ ($M_\odot$ kpc^{-2}) (9)	ext$_r$ (mag) (10)	r (mag) (11)	(b/a)$_r$ (12)	incl (deg) (13)	NUV$-r$ (mag) (14)	T$_{NUV}$ (sec) (15)	$T_{\max}$ (min) (16)
38546	J141229.86+111425.9	UGC9089	0.0282	11.03	6.73	7.47	18.52	9.02	0.06	13.56	0.382	71	4.37	106	2
41444	J141547.01+085436.6	...	0.0287	10.73	2.18	2.25	7.20	9.69	0.07	14.22	0.630	52	5.32	222	8
45439	J141722.70+250310.1	CGCG133-024	0.0299	10.90	3.52	3.63	11.33	9.40	0.05	14.00	0.459	65	5.69	28617	5
30854	J141833.16+071712.4	...	0.0257	10.16	5.86	6.33	17.52	8.36	0.09	15.59	0.197	90	4.50	1680	15
30847	J141835.33+072118.8	...	0.0250	10.29	3.40	3.51	10.16	8.98	0.08	14.86	0.416	68	5.59	1680	14
28875	J143041.62+115913.3	...	0.0271	10.39	2.76	2.83	8.19	9.19	0.07	14.80	0.769	41	5.83	107	19
7520	J143314.34+023909.6	CGCG047-087	0.0291	10.80	4.92	5.50	15.45	9.04	0.10	14.25	0.411	68	5.66	1690	6
9601	J143351.42+034046.1	CGCG047-095	0.0288	10.83	3.67	3.84	12.20	9.33	0.10	14.18	0.538	59	6.09	1696	5
9585	J143419.01+033951.7	CGCG047-101	0.0336	11.04	4.47	5.01	16.47	9.23	0.10	13.95	0.572	57	4.45	1696	4
46068	J143709.53+251503.0	CGCG133-098	0.0340	11.40	5.03	5.99	17.60	9.48	0.08	13.88	0.538	59	5.59	90	1
41703	J144119.18+085256.5	...	0.0294	10.16	2.98	3.04	9.44	8.82	0.07	15.34	0.569	57	3.71	208	27
29205	J144551.55+100910.4	...	0.0375	10.11	3.29	4.08	9.34	8.47	0.07	16.44	0.286	78	3.21	299	72
29225	J144636.62+115108.7	...	0.0294	10.40	2.84	2.89	8.35	9.11	0.08	15.07	0.619	53	5.45	281	27
38732	J145033.16+093742.2	CGCG076-071	0.0499	11.08	3.50	3.50	10.89	9.13	0.08	14.41	0.924	23	5.72	11717	17
38728	J145055.60+093946.5	...	0.0386	10.08	1.32	1.38	4.42	9.21	0.09	16.21	0.722	45	5.19	144	82
38706	J145129.30+092005.9	UGC9561	0.0293	10.96	4.02	5.10	14.64	9.36	0.09	13.80	0.517	61	4.28	11717	3
10012	J145243.07+031329.3	CGCG048-044	0.0279	10.76	3.48	3.74	12.72	9.33	0.12	13.96	0.685	48	5.55	5768	7
10058	J145413.13+045029.5	IC1072	0.0347	11.06	5.55	6.04	19.15	9.03	0.10	13.78	0.640	52	5.68	3652	4
41783	J145730.93+082326.3	CGCG076-111	0.0371	11.09	3.18	3.29	10.12	9.49	0.10	13.93	0.524	60	4.58	141	5
38923	J145758.08+110027.4	CGCG076-114	0.0479	11.04	4.92	5.28	14.07	8.83	0.10	14.27	0.738	43	3.55	64	16
41793	J145841.32+075905.9	CGCG048-086	0.0376	11.25	7.25	8.35	19.82	8.92	0.09	13.56	0.813	36	5.38	149	2
39120	J150935.51+102525.9	...	0.0276	10.26	3.44	3.69	10.23	8.86	0.10	15.63	0.266	80	4.00	201	20
38974	J151133.48+092824.2	CGCG077-036	0.0353	11.17	4.82	6.22	21.45	9.26	0.11	14.02	0.666	50	5.97	144	3
10297	J151252.96+043050.4	CGCG049-043	0.0370	11.14	3.15	3.24	10.82	9.55	0.14	13.74	0.707	46	5.75	1408	4
39211	J151435.92+082002.1	CGCG077-049	0.0334	11.03	3.38	3.49	11.40	9.47	0.08	13.69	0.492	63	5.61	135	4
42011	J151615.35+064747.5	CGCG049-081	0.0343	10.78	3.15	3.23	9.83	9.26	0.10	14.43	0.531	60	5.81	1696	14
42174	J151817.19+070757.0	...	0.0320	10.34	2.25	2.29	6.63	9.17	0.10	15.33	0.610	54	5.69	2261	38
46564	J151925.35+254713.6	CGCG135-046	0.0323	11.05	4.15	4.45	14.31	9.34	0.13	13.90	0.761	41	5.50	261	3
39600	J152750.23+094002.2	...	0.0436	10.72	2.78	2.84	8.38	9.09	0.10	15.16	0.483	63	5.19	107	49
46678	J153339.97+242416.8	CGCG136-012	0.0434	11.19	5.66	6.52	22.01	8.95	0.15	13.97	0.912	25	4.73	175	5
42287	J154245.88+245909.9	CGCG136-062	0.0336	11.19	5.29	5.86	18.15	9.23	0.12	13.45	0.659	50	4.70	172	2
10827	J220147.39+131228.5	...	0.0301	10.11	2.76	2.84	7.82	8.81	0.18	15.65	0.581	56	6.50	208	29
10831	J220322.59+123857.6	CGCG428-021	0.0273	10.46	3.50	3.71	10.11	9.05	0.16	14.80	0.516	61	5.00	186	20
10856	J220330.28+123938.9	NGC7195	0.0264	10.78	4.23	4.45	12.88	9.24	0.16	13.94	0.780	40	5.41	186	5
10813	J220358.03+115421.2	...	0.0268	10.55	3.70	3.92	12.05	9.11	0.46	14.62	0.811	37	5.47	186	14
10836	J220419.41+125806.2	CGCG428-026	0.0274	10.69	3.53	3.79	12.43	9.27	0.15	14.28	0.564	57	6.28	208	8
10850	J220538.79+122521.3	...	0.0355	10.28	3.30	3.41	8.16	8.69	0.25	15.76	0.325	75	4.00	186	58
10863	J220848.81+132152.9	...	0.0275	10.48	3.20	3.56	10.93	9.14	0.20	15.13	0.389	70	5.57	208	20
10841	J221111.69+114802.6	...	0.0270	10.36	3.15	3.40	9.37	9.05	0.22	14.66	0.676	49	3.68	3264	19
10885	J221212.48+121218.6	...	0.0275	10.04	4.06	4.25	8.98	8.49	0.18	14.83	0.787	39	2.51	2790	20
10889	J221236.07+140103.9	...	0.0266	10.45	3.23	3.76	12.67	9.14	0.17	14.83	0.832	34	5.15	7104	18
10890	J221241.31+140434.4	...	0.0252	10.35	4.98	5.67	16.23	8.71	0.17	14.66	0.869	30	5.26	7104	14
10844	J221253.09+122158.7	...	0.0271	10.16	2.37	2.50	7.23	9.10	0.17	15.36	0.727	44	5.62	2790	19
10896	J221336.49+134020.7	...	0.0278	10.13	3.18	3.26	8.16	8.79	0.17	15.35	0.571	57	5.56	7104	21
10942	J221530.28+134023.4	...	0.0251	10.04	2.32	2.43	7.92	9.06	0.18	15.44	0.828	35	5.54	7104	14
10943	J221540.59+133616.9	...	0.0275	10.23	3.90	4.13	9.93	8.71	0.19	15.17	0.531	60	5.00	7104	20
10944	J221543.66+134252.3	...	0.0262	10.05	1.75	1.85	5.99	9.28	0.19	15.45	0.616	53	5.51	7104	17

Table A.1. continued.

GASS (1)	SDSS ID (2)	Other name (3)	z_{SDSS} (4)	Log $M_\star$ ($M_\odot$) (5)	$R_{50,z}$ ($''$) (6)	R_{50} ($''$) (7)	R_{90} ($''$) (8)	Log $\mu_\star$ ($M_\odot$ kpc^{-2}) (9)	ext$_r$ (mag) (10)	r (mag) (11)	(b/a)$_r$ (12)	incl (deg) (13)	NUV$-r$ (mag) (14)	T$_{NUV}$ (sec) (15)	$T_{\max}$ (min) (16)
10950	J221559.51+132715.3	...	0.0254	10.21	1.82	1.86	4.98	9.43	0.19	15.18	0.677	49	5.65	7104	15
10949	J221600.51+130851.8	...	0.0262	10.33	2.59	2.67	8.98	9.21	0.20	14.79	0.350	73	5.43	1696	17
10948	J221636.89+131514.4	...	0.0258	10.02	3.53	4.12	10.31	8.65	0.20	15.82	0.356	73	4.82	1696	16
10953	J221652.39+132533.5	...	0.0256	10.21	2.94	2.94	8.57	9.01	0.21	14.98	0.390	70	5.55	1696	15
10952	J221657.95+133235.0	...	0.0262	10.47	4.04	4.45	11.49	8.97	0.20	15.07	0.280	78	7.13	173	17
10879	J221750.25+125941.7	...	0.0360	10.05	1.17	1.20	3.53	9.34	0.24	16.31	0.735	44	5.11	1670	61
10979	J221859.40+131114.8	CGCG428-072	0.0268	10.33	2.64	2.67	9.74	9.18	0.23	14.72	0.729	44	4.99	1670	18
10990	J223137.59+130343.2	...	0.0367	10.36	4.68	4.93	11.47	8.43	0.18	16.06	0.123	90	2.81	199	66
10985	J223407.83+123415.9	...	0.0495	10.78	3.13	4.39	10.91	8.94	0.15	15.71	0.568	57	4.28	207	61
11013	J223650.63+143055.6	...	0.0358	10.20	4.43	4.78	9.58	8.34	0.20	15.40	0.742	43	3.22	3001	60
11015	J223701.58+142417.4	...	0.0367	10.76	4.19	4.72	14.69	8.93	0.19	14.63	0.634	52	5.51	31414	20
11003	J223715.17+141551.3	...	0.0367	10.29	2.78	3.01	7.24	8.82	0.17	15.81	0.335	74	4.05	31414	66
11019	J223810.59+142626.1	...	0.0360	10.05	3.72	3.76	7.82	8.34	0.19	16.13	0.319	75	3.63	3141	61
11041	J224237.97+132844.5	...	0.0373	10.03	2.81	3.05	8.53	8.53	0.13	16.28	0.940	20	5.71	11561	71
11055	J225026.03+145510.3	...	0.0275	10.45	4.69	5.11	14.00	8.78	0.17	14.46	0.815	36	3.94	199	20
11087	J225525.96+125539.3	...	0.0376	10.88	3.62	3.80	11.60	9.16	0.12	14.86	0.325	75	5.28	2905	13
11071	J225726.69+130005.9	...	0.0257	10.56	6.24	7.08	16.92	8.70	0.19	14.28	0.571	57	4.40	2905	12
11126	J230111.07+130932.5	...	0.0484	10.75	4.00	4.08	9.74	8.71	0.56	14.96	0.571	57	3.66	1610	65
11132	J230146.58+133218.8	...	0.0341	10.62	2.12	2.16	7.11	9.45	0.36	14.64	0.542	59	6.21	1610	28
11231	J230307.96+135327.4	...	0.0341	10.06	4.99	5.58	11.55	8.14	0.39	15.26	0.436	67	2.97	1610	49
11120	J230343.06+135535.5	...	0.0271	10.40	3.56	3.88	10.23	8.99	0.42	14.55	0.367	72	3.49	1687	19
11250	J230735.69+152754.1	...	0.0364	10.30	4.04	4.19	9.88	8.51	0.56	15.42	0.414	68	3.85	298	64
11268	J231138.88+150741.6	...	0.0418	10.72	2.83	3.35	10.05	9.11	0.29	15.17	0.870	30	3.47	3284	42
11267	J231142.06+150638.2	CGCG431-010	0.0400	11.07	5.00	5.49	13.09	9.01	0.27	14.06	0.816	36	4.06	3284	7
11314	J231224.51+135704.5	...	0.0341	10.54	3.02	3.28	9.36	9.06	0.19	14.89	0.595	55	4.19	3264	40
11297	J231331.44+141938.6	...	0.0392	10.41	1.88	1.85	6.28	9.22	0.17	15.07	0.856	32	5.44	4965	87
11303	J231340.50+131331.8	...	0.0395	10.35	3.76	4.12	10.06	8.55	0.16	16.38	0.200	90	4.30	3264	90
11285	J231516.82+133201.6	...	0.0395	10.05	2.27	2.51	6.48	8.69	0.15	16.95	0.218	85	4.80	3335	89
11280	J231530.93+134040.6	...	0.0400	10.99	5.22	5.61	19.00	8.89	0.17	14.36	0.560	58	5.28	3335	10
11462	J231756.35+135352.1	...	0.0395	10.90	3.66	4.20	14.65	9.12	0.14	14.47	0.572	57	4.37	2256	15
11270	J231816.95+133426.6	...	0.0395	10.07	2.32	2.41	6.93	8.69	0.15	16.23	0.639	52	3.91	3335	90
11349	J231836.21+151758.7	...	0.0256	10.13	4.99	5.52	12.09	8.47	0.11	14.76	0.523	60	2.88	4851	15
11437	J232215.37+140450.6	...	0.0264	10.56	4.35	5.05	13.73	8.99	0.13	14.55	0.368	72	3.83	1676	13
11513	J232239.48+154405.3	...	0.0411	10.62	4.19	4.47	9.65	8.68	0.11	15.32	0.772	40	4.53	3180	62
11514	J232326.53+152510.4	...	0.0428	10.27	1.56	1.65	4.91	9.16	0.14	16.27	0.643	51	4.27	3180	124
11494	J232335.34+151148.8	...	0.0427	10.62	4.22	4.65	9.63	8.65	0.21	15.09	0.614	54	2.95	3180	71
11397	J232447.10+142301.6	...	0.0395	10.46	2.01	2.06	6.59	9.21	0.11	15.52	0.870	30	5.22	1681	89
11383	J232548.27+140317.2	...	0.0377	10.21	3.01	3.29	8.49	8.65	0.13	15.78	0.643	51	3.23	2434	74
11366	J232621.83+141230.1	...	0.0430	10.87	3.38	3.55	9.86	9.09	0.14	14.74	0.663	50	5.47	2434	23
11357	J232624.38+135742.9	...	0.0433	10.87	3.22	3.36	10.07	9.12	0.14	14.88	0.446	66	5.81	2434	24
11582	J232748.74+142831.1	...	0.0411	10.86	3.83	4.41	11.90	9.00	0.18	14.86	0.710	46	5.56	2932	20
11687	J232753.17+144239.5	...	0.0416	10.92	2.88	3.15	10.61	9.30	0.21	14.86	0.772	40	5.55	2932	16
11697	J233113.42+151402.9	...	0.0312	10.02	2.97	3.38	9.17	8.64	0.17	16.42	0.442	66	3.88	2473	34
11727	J233341.93+140429.8	...	0.0328	10.40	1.88	2.21	7.32	9.37	0.22	15.45	0.864	31	5.32	2327	42
11763	J234157.75+151407.2	...	0.0256	10.21	2.30	2.43	6.94	9.22	0.10	15.94	0.270	79	4.59	2963	15
11770	J234646.15+160235.0	CGCG455-046	0.0416	11.31	4.94	5.45	16.52	9.22	0.08	13.93	0.785	39	5.14	247	3
11754	J234823.35+143004.8	...	0.0409	10.77	3.26	3.57	10.06	9.06	0.11	15.00	0.606	54	5.56	2942	29

Table A.1. continued.

GASS (1)	SDSS ID (2)	Other name (3)	$z_{\rm SDSS}$ (4)	Log $M_\star$ ($M_\odot$) (5)	$R_{50,z}$ ($''$) (6)	R_{50} ($''$) (7)	R_{90} ($''$) (8)	Log $\mu_\star$ ($M_\odot$ kpc^{-2}) (9)	ext$_r$ (mag) (10)	r (mag) (11)	(b/a)$_r$ (12)	incl (deg) (13)	NUV$-r$ (mag) (14)	T$_{NUV}$ (sec) (15)	$T_{\rm max}$ (min) (16)
11783	J235224.35+143535.1	...	0.0270	10.33	2.22	2.37	6.66	9.33	0.10	15.02	0.745	43	5.58	1699	19
11808	J235257.31+154244.8	...	0.0479	10.78	4.28	4.56	11.90	8.69	0.11	14.97	0.678	49	4.97	1693	55
11815	J235308.28+160351.9	CGCG455-064	0.0491	11.12	2.79	3.06	10.14	9.38	0.11	14.56	0.715	46	4.99	3673	13
11845	J235644.47+135435.4	...	0.0363	10.60	4.90	5.32	13.15	8.65	0.16	14.98	0.347	73	4.10	1705	39
11824	J235747.57+153649.2	...	0.0380	10.25	6.17	6.33	14.09	8.05	0.14	15.46	0.486	63	3.24	1677	76

Table A.2. HI Properties of GASS Detections.

GASS (1)	SDSS ID (2)	z_{SDSS} (3)	T_{on} (min) (4)	Δv (km s^{-1}) (5)	z (6)	W_{50} (km s^{-1}) (7)	$W_{50}{}^{c}$ (km s^{-1}) (8)	F (Jy km s^{-1}) (9)	rms (mJy) (10)	S/N (11)	Log M_{HI} ($M_\odot$) (12)	Log $M_{HI}/M_\star$ (13)	Q (14)
11834	J000047.89+141639.1	0.0362	4	15	0.036162	380± 16	359	0.72± 0.12	0.67	10.0	9.62	−1.09	1*
11825	J000210.19+140810.3	0.0420	43	21	0.042186	419± 14	392	0.23± 0.04	0.19	8.8	9.26	−1.36	1
11917	J000742.65+151112.7	0.0446	25	13	0.044594	401± 3	378	0.43± 0.05	0.30	14.0	9.58	−1.16	5*
3163	J002846.83+150529.3	0.0422	15	21	0.042253	394± 2	368	0.48± 0.07	0.32	11.5	9.58	−1.05	1
3151	J003143.05+142911.2	0.0381	76	13	0.038243	328± 9	309	0.13± 0.02	0.15	9.5	8.93	−1.47	1
27181	J003248.17+144738.1	0.0418	5	21	0.041922	297± 12	275	0.44± 0.09	0.50	7.9	9.53	−1.07	1
27167	J003921.66+142811.5	0.0380	5	21	0.038093	246± 13	227	0.62± 0.10	0.56	10.9	9.60	−0.77	1*
3189	J004023.48+143649.4	0.0384	9	16	0.038583	412± 13	389	0.83± 0.08	0.44	16.6	9.74	−0.31	1*
27219	J004125.29+134334.3	0.0332	19	15	0.033323	339± 5	320	0.30± 0.05	0.31	9.6	9.17	−1.04	1
3233	J005134.04+135452.7	0.0392	10	16	0.039274	266± 3	248	0.28± 0.06	0.39	7.8	9.27	−0.95	1
3439	J010905.96+144520.8	0.0386	10	13	0.038540	301± 2	284	0.54± 0.07	0.47	13.2	9.55	−0.80	1*
3465	J011221.82+150039.0	0.0292	15	13	0.029224	287± 5	273	0.70± 0.06	0.41	19.9	9.42	−0.77	1*
3509	J011711.65+132027.3	0.0484	35	21	0.048353	444± 15	413	0.28± 0.05	0.21	9.1	9.47	−1.34	1*
3524	J011716.09+143720.5	0.0380	25	16	0.038096	393± 15	371	0.43± 0.06	0.30	12.9	9.44	−1.29	1
3519	J011728.11+144215.9	0.0427	10	16	0.042766	296± 6	276	0.42± 0.07	0.43	10.2	9.53	−1.22	1*
3819	J014143.18+134032.8	0.0453	4	16	0.045365	222± 10	205	0.95± 0.09	0.61	18.6	9.94	−0.73	1
4203	J015027.35+141140.0	0.0341	10	13	0.033997	322± 2	305	0.65± 0.06	0.39	18.2	9.52	−0.66	1
4145	J015517.63+125935.5	0.0322	14	15	0.031855	337± 19	319	0.56± 0.06	0.32	16.9	9.40	−0.90	1*
4137	J015651.99+131246.0	0.0445	15	21	0.044561	240± 25	220	0.40± 0.05	0.31	12.6	9.54	−1.36	1*
4233	J015707.32+145543.5	0.0433	5	16	0.043363	147± 13	134	0.54± 0.08	0.68	11.6	9.65	−1.23	5*
4223	J015712.97+144407.6	0.0260	8	21	0.025948	429± 25	408	0.99± 0.10	0.43	16.8	9.47	−1.09	1*
3918	J015718.40+130745.8	0.0327	40	15	0.032759	138± 35	127	0.12± 0.02	0.21	8.7	8.75	−1.62	1*
4017	J020517.54+133020.6	0.0258	5	13	0.025801	130± 3	121	0.62± 0.06	0.68	16.0	9.25	−0.98	1
3977	J020744.46+140453.7	0.0324	5	13	0.032482	294± 1	278	0.70± 0.11	0.73	11.1	9.51	−0.75	1*
4030	J020939.47+135859.4	0.0491	5	16	0.049204	137± 4	123	0.38± 0.07	0.61	9.5	9.61	−1.72	1*
4038	J021121.82+143015.5	0.0417	5	16	0.041729	445± 29	419	1.14± 0.11	0.58	15.8	9.94	−0.78	1*
4039	J021131.43+141202.4	0.0254	10	12	0.025428	308± 5	294	1.11± 0.07	0.49	25.8	9.50	−0.82	1*
4048	J021219.38+133645.6	0.0414	10	16	0.041399	359± 8	337	0.71± 0.08	0.46	14.6	9.73	−0.82	1*
3981	J021404.39+131156.3	0.0416	35	16	0.041766	426± 4	402	0.27± 0.04	0.23	9.9	9.32	−1.23	1*
4057	J021419.24+135611.2	0.0397	10	13	0.039734	350± 14	330	1.13± 0.09	0.57	21.0	9.90	−0.62	1*
56304	J080534.10+102336.2	0.0340	4	13	0.034007	324± 1	308	1.67± 0.12	0.81	22.6	9.93	−0.96	1*
56632	J090437.07+133314.7	0.0281	9	21	0.028390	744± 10	713	0.68± 0.10	0.34	8.4	9.38	−1.62	2*
16753	J091828.43+062003.7	0.0335	40	13	0.033520	113± 4	103	0.08± 0.02	0.22	6.6	8.58	−1.71	1
18702	J095051.58+081340.7	0.0299	15	15	0.029881	348± 4	330	0.48± 0.07	0.41	11.1	9.27	−0.93	1*
18707	J095150.14+082213.8	0.0405	8	13	0.040481	314± 4	296	0.74± 0.09	0.57	14.5	9.73	−0.84	1*
18673	J095301.79+072736.4	0.0385	25	21	0.038467	374± 2	350	0.33± 0.05	0.24	11.0	9.33	−1.05	1*
18686	J095302.62+075029.3	0.0411	5	13	0.041025	363± 8	342	2.74± 0.10	0.61	46.2	10.31	−0.24	1*
18681	J095324.56+074956.2	0.0393	14	16	0.039384	443± 8	419	0.73± 0.08	0.39	15.1	9.70	−0.97	1*
20292	J095349.23+091137.6	0.0299	13	15	0.029884	335± 15	318	0.40± 0.07	0.39	10.3	9.20	−1.47	1*
20448	J095812.59+110635.5	0.0272	10	13	0.027312	281± 3	267	0.71± 0.06	0.46	18.4	9.37	−0.69	1*
5035	J100152.69+030040.7	0.0441	15	21	0.044017	391± 50	364	0.43± 0.07	0.32	10.4	9.57	−1.20	1*
18830	J101100.68+085920.7	0.0320	19	15	0.032102	308± 2	291	0.27± 0.05	0.29	9.5	9.08	−1.19	1
18798	J101329.66+075415.5	0.0458	10	21	0.045521	692± 37	651	0.48± 0.10	0.36	5.8	9.64	−1.58	3*
18877	J102025.15+074037.8	0.0452	15	13	0.045315	501± 1	473	0.45± 0.08	0.42	8.5	9.61	−1.36	1
18887	J102055.54+081849.4	0.0458	15	16	0.045745	529± 7	499	0.62± 0.08	0.38	10.9	9.76	−1.00	1
26320	J102238.71+120517.8	0.0450	20	16	0.044981	538± 2	508	0.42± 0.07	0.32	8.7	9.58	−1.13	1
18862	J102241.20+082003.2	0.0446	15	16	0.044718	410± 24	385	0.54± 0.07	0.39	12.0	9.68	−1.00	1*

Table A.2. continued.

GASS (1)	SDSS ID (2)	z_{SDSS} (3)	T_{on} (min) (4)	Δv (km s^{-1}) (5)	z (6)	W_{50} (km s^{-1}) (7)	$W_{50}{}^{c}$ (km s^{-1}) (8)	F (Jy km s^{-1}) (9)	rms (mJy) (10)	S/N (11)	Log M_{HI} (M$_\odot$) (12)	Log $M_{HI}/M_\star$ (13)	Q (14)
23026	J102721.97+110447.9	0.0323	4	21	0.032379	616± 4	587	0.96± 0.16	0.58	8.3	9.65	−1.51	1*
26570	J103905.90+132153.5	0.0325	30	15	0.032442	217± 20	202	0.16± 0.03	0.23	8.6	8.87	−1.13	1
23227	J103913.15+121130.9	0.0479	10	13	0.047943	592± 3	559	1.10± 0.11	0.52	13.8	10.05	−1.13	1
15211	J104024.66+065137.7	0.0303	5	13	0.030338	483± 5	462	1.73± 0.12	0.64	22.2	9.84	−1.05	1*
26639	J104046.05+134659.9	0.0317	40	21	0.031915	428± 22	405	0.15± 0.04	0.19	5.7	8.82	−1.42	3*
15166	J104121.14+061644.3	0.0339	8	13	0.033913	185± 2	172	0.61± 0.08	0.67	13.3	9.49	−0.53	1*
29555	J104145.56+135352.9	0.0316	15	15	0.031649	322± 8	304	0.40± 0.05	0.32	12.5	9.24	−1.14	1*
57099	J104221.91+152134.6	0.0490	10	16	0.049017	192± 16	176	0.31± 0.06	0.46	8.6	9.52	−1.58	1*
15151	J104251.39+055135.5	0.0334	8	15	0.033316	459± 11	437	0.94± 0.11	0.57	12.9	9.66	−1.33	1*
29624	J110050.33+133551.4	0.0340	9	15	0.034080	317± 6	299	0.78± 0.08	0.48	16.5	9.60	−0.72	1
47896	J110851.20+282832.5	0.0363	4	13	0.036432	480± 13	457	3.17± 0.15	0.82	32.0	10.27	−0.85	1
12318	J111443.35+040128.2	0.0417	8	21	0.041272	469± 1	440	0.39± 0.09	0.38	6.6	9.46	−1.75	2*
12293	J112029.23+040742.1	0.0496	5	21	0.049618	553± 3	516	0.53± 0.14	0.54	5.4	9.76	−1.56	2
29892	J112946.35+152001.1	0.0366	5	21	0.036976	695± 11	660	1.31± 0.15	0.51	11.3	9.90	−1.12	5*
23757	J113645.51+132009.9	0.0342	15	15	0.034140	394± 26	374	0.40± 0.06	0.34	10.7	9.32	−1.19	1*
18087	J114940.66+094255.1	0.0352	30	15	0.035221	312± 1	294	0.17± 0.04	0.23	7.5	8.97	−1.42	1*
24168	J121612.36+132615.4	0.0260	15	13	0.026108	459± 8	442	0.89± 0.07	0.38	20.3	9.42	−1.02	1
28057	J122532.62+080301.4	0.0381	10	13	0.038136	221± 2	207	0.38± 0.06	0.49	10.3	9.39	−0.91	1
18576	J123625.93+085639.7	0.0277	24	21	0.027709	328± 4	309	0.18± 0.05	0.24	6.2	8.77	−1.49	1
24437	J123949.27+133256.8	0.0466	10	13	0.046425	552± 22	521	1.93± 0.10	0.50	27.2	10.27	−0.40	5*
28482	J124307.28+111243.1	0.0282	5	13	0.028183	357± 3	341	1.70± 0.11	0.70	25.8	9.77	−0.46	5*
25167	J130256.89+125250.0	0.0362	10	13	0.036205	432± 2	411	0.92± 0.08	0.48	17.5	9.72	−0.77	1
40425	J130404.23+084820.6	0.0358	4	15	0.035708	316± 11	297	0.72± 0.11	0.69	10.5	9.61	−0.56	1*
13158	J130454.21+034928.1	0.0410	10	10	0.040918	246± 12	231	1.69± 0.07	0.61	39.0	10.10	−0.71	1*
6749	J130750.80+031140.7	0.0386	9	16	0.038443	462± 5	438	1.03± 0.11	0.56	14.3	9.83	−1.29	1*
25296	J132357.45+120233.3	0.0390	8	21	0.039157	536± 4	505	0.89± 0.11	0.44	11.8	9.78	−1.23	1*
51190	J134404.06+253948.6	0.0486	10	16	0.048554	515± 26	484	1.07± 0.09	0.41	18.1	10.05	−0.98	1*
13624	J135152.41+032718.0	0.0296	5	13	0.029634	294± 1	279	4.09± 0.11	0.76	62.9	10.20	−0.11	1
44846	J135512.58+250117.1	0.0310	4	15	0.031065	339± 3	321	0.72± 0.12	0.70	10.2	9.49	−1.51	1*
40260	J135827.10+132904.7	0.0388	25	21	0.039140	683± 4	647	0.43± 0.07	0.25	7.8	9.47	−1.30	5*
41303	J140741.05+094835.8	0.0374	20	16	0.037573	184± 6	170	0.15± 0.04	0.29	6.7	8.96	−1.27	5*
38538	J141119.35+113105.1	0.0385	45	16	0.038607	170± 3	156	0.14± 0.03	0.22	8.8	8.97	−1.16	1*
38546	J141229.86+111425.9	0.0282	8	15	0.028260	529± 19	507	0.83± 0.11	0.53	10.8	9.47	−1.56	1
30854	J141833.16+071712.4	0.0257	15	13	0.025698	327± 4	313	0.64± 0.06	0.38	19.0	9.27	−0.89	1*
7520	J143314.34+023909.6	0.0291	15	21	0.029100	462± 40	438	0.64± 0.08	0.36	12.0	9.37	−1.43	1*
9585	J143419.01+033951.7	0.0336	8	21	0.033633	561± 1	533	0.51± 0.13	0.49	5.7	9.40	−1.64	3*
46068	J143709.53+251503.0	0.0340	4	21	0.034030	705± 9	672	0.93± 0.17	0.58	7.1	9.68	−1.72	1*
41703	J144119.18+085256.5	0.0294	28	21	0.029490	247± 15	230	0.12± 0.04	0.23	5.2	8.66	−1.50	2
29205	J144551.55+100910.4	0.0375	15	16	0.037553	326± 5	307	0.45± 0.06	0.34	13.0	9.44	−0.67	1
38732	J145033.16+093742.2	0.0499	18	21	0.050228	494± 5	460	0.28± 0.08	0.32	5.4	9.49	−1.59	3*
38706	J145129.30+092005.9	0.0293	5	15	0.029310	173± 51	160	0.57± 0.10	0.67	11.9	9.33	−1.63	5*
41783	J145730.93+082326.3	0.0371	10	21	0.037032	587± 65	556	0.83± 0.10	0.37	11.7	9.70	−1.39	2*
38923	J145758.08+110027.4	0.0479	20	16	0.047967	429± 3	402	0.47± 0.07	0.34	11.3	9.68	−1.36	1*
41793	J145841.32+075905.9	0.0376	4	27	0.037633	350± 7	324	0.32± 0.11	0.47	4.9	9.30	−1.95	3*
46678	J153339.97+242416.8	0.0434	10	21	0.043497	249± 2	229	0.26± 0.08	0.44	5.7	9.33	−1.86	2
42287	J154245.88+245909.9	0.0336	4	21	0.033703	588± 1	558	0.86± 0.18	0.67	6.8	9.64	−1.55	1*
10831	J220322.59+123857.6	0.0273	10	15	0.026895	700± 41	675	2.51± 0.13	0.52	25.0	9.90	−0.56	5*

Table A.2. continued.

GASS (1)	SDSS ID (2)	z_{SDSS} (3)	T_{on} (min) (4)	Δv (km s^{-1}) (5)	z (6)	W_{50} (km s^{-1}) (7)	$W_{50}{}^{c}$ (km s^{-1}) (8)	F (Jy km s^{-1}) (9)	rms (mJy) (10)	S/N (11)	Log M_{HI} (M$_\odot$) (12)	Log $M_{HI}/M_\star$ (13)	Q (14)
10856	J220330.28+123938.9	0.0264	5	13	0.026538	465± 13	446	2.82± 0.14	0.76	31.9	9.94	−0.84	5*
10850	J220538.79+122521.3	0.0355	10	15	0.035461	298± 18	281	0.54± 0.08	0.48	11.7	9.48	−0.80	1*
10841	J221111.69+114802.6	0.0270	5	15	0.027039	308± 10	292	0.63± 0.09	0.58	11.2	9.30	−1.06	1
10885	J221212.48+121218.6	0.0275	15	13	0.027579	208± 3	196	0.39± 0.05	0.42	12.9	9.11	−0.93	1
10889	J221236.07+140103.9	0.0266	10	15	0.026598	310± 14	295	1.04± 0.07	0.44	24.7	9.51	−0.94	5*
10844	J221253.09+122158.7	0.0271	10	13	0.026999	146± 8	137	0.33± 0.05	0.48	11.2	9.02	−1.14	5*
10990	J223137.59+130343.2	0.0367	10	13	0.036785	396± 2	376	1.16± 0.09	0.53	21.7	9.84	−0.52	1
10985	J223407.83+123415.9	0.0495	15	13	0.049508	408± 7	383	0.98± 0.07	0.42	22.3	10.03	−0.76	1*
11013	J223650.63+143055.6	0.0358	10	15	0.035815	298± 16	280	0.44± 0.07	0.41	11.3	9.40	−0.80	1*
11015	J223701.58+142417.4	0.0367	5	15	0.036475	528± 4	502	1.24± 0.13	0.62	13.6	9.86	−0.90	5*
11003	J223715.17+141551.3	0.0367	25	16	0.037393	679± 12	647	1.05± 0.06	0.26	21.1	9.81	−0.48	5*
11019	J223810.59+142626.1	0.0360	59	21	0.036002	299± 14	279	0.12± 0.03	0.16	6.8	8.83	−1.22	2*
11055	J225026.03+145510.3	0.0275	14	15	0.027429	39± 21	31	0.17± 0.03	0.38	13.2	8.76	−1.69	1*
11071	J225726.69+130005.9	0.0257	13	15	0.025744	254± 15	240	0.36± 0.05	0.36	11.2	9.01	−1.55	1*
11126	J230111.07+130932.5	0.0484	14	16	0.048330	343± 8	319	0.40± 0.07	0.39	9.8	9.62	−1.13	1*
11231	J230307.96+135327.4	0.0341	5	13	0.034084	262± 3	247	0.78± 0.10	0.70	13.6	9.60	−0.46	1*
11120	J230343.06+135535.5	0.0271	19	21	0.027092	475± 81	453	0.33± 0.07	0.28	7.6	9.02	−1.38	3*
11250	J230735.69+152754.1	0.0364	14	15	0.036288	434± 4	412	0.38± 0.07	0.38	8.2	9.34	−0.96	1*
11268	J231138.88+150741.6	0.0418	20	16	0.041826	385± 14	362	0.48± 0.06	0.33	13.3	9.57	−1.15	1*
11314	J231224.51+135704.5	0.0341	10	15	0.034174	480± 17	457	1.09± 0.10	0.48	17.0	9.75	−0.79	5*
11297	J231331.44+141938.6	0.0392	89	21	0.039457	481± 11	453	0.12± 0.03	0.14	5.5	8.92	−1.49	3
11303	J231340.50+131331.8	0.0395	25	16	0.039544	325± 23	305	0.35± 0.05	0.32	10.7	9.38	−0.97	1*
11285	J231516.82+133201.6	0.0395	90	21	0.039437	345± 18	322	0.13± 0.03	0.12	8.5	8.94	−1.11	1*
11462	J231756.35+135352.1	0.0395	10	13	0.039694	472± 2	448	0.92± 0.08	0.46	16.7	9.81	−1.09	1*
11270	J231816.95+133426.6	0.0395	90	21	0.039554	304± 17	283	0.07± 0.02	0.12	5.1	8.70	−1.37	3*
11349	J231836.21+151758.7	0.0256	15	21	0.025684	251± 10	235	0.39± 0.06	0.35	11.1	9.06	−1.07	1
11437	J232215.37+140450.6	0.0264	5	13	0.026398	371± 7	356	0.87± 0.11	0.66	13.6	9.42	−1.14	1
11513	J232239.48+154405.3	0.0411	62	21	0.041302	216± 11	197	0.07± 0.03	0.16	4.7	8.75	−1.87	3*
11514	J232326.53+152510.4	0.0428	90	21	0.042826	337± 11	313	0.10± 0.03	0.16	5.4	8.91	−1.36	3*
11494	J232335.34+151148.8	0.0427	13	13	0.042806	324± 3	304	0.48± 0.06	0.40	13.2	9.59	−1.03	1
11383	J232548.27+140317.2	0.0377	18	16	0.037743	256± 14	239	0.25± 0.05	0.33	8.7	9.20	−1.01	1*
11687	J232753.17+144239.5	0.0416	25	16	0.041692	588± 4	557	0.28± 0.06	0.27	6.5	9.34	−1.58	1
11697	J233113.42+151402.9	0.0312	15	13	0.031198	297± 9	282	0.33± 0.06	0.39	9.8	9.15	−0.87	1
11727	J233341.93+140429.8	0.0328	43	15	0.032893	271± 1	254	0.10± 0.03	0.21	5.3	8.68	−1.72	3
11763	J234157.75+151407.2	0.0256	13	12	0.025548	298± 4	284	1.16± 0.06	0.41	32.9	9.52	−0.69	5*
11808	J235257.31+154244.8	0.0479	45	21	0.048033	421± 11	392	0.19± 0.05	0.21	6.6	9.29	−1.49	3*
11815	J235308.28+160351.9	0.0491	13	21	0.048924	889± 3	837	0.87± 0.11	0.33	9.1	9.97	−1.15	5*
11845	J235644.47+135435.4	0.0363	5	21	0.036522	288± 22	268	1.20± 0.10	0.54	20.2	9.85	−0.75	5*
11824	J235747.57+153649.2	0.0380	9	16	0.037973	306± 8	288	0.54± 0.09	0.52	10.5	9.53	−0.72	1*

Table A.3. GASS Non-detections.

GASS (1)	SDSS ID (2)	z_{SDSS} (3)	T_{on} (min) (4)	rms (mJy) (5)	Log $M_{HI,lim}$ ($M_\odot$) (6)	Log $M_{HI,lim}/M_\star$ (7)	Note (8)
12005	J002420.72+144632.3	0.0309	35	0.21	8.62	−1.44	*
12002	J002504.00+145815.2	0.0367	65	0.17	8.68	−1.80	*
3301	J005915.31+133433.3	0.0404	16	0.33	9.07	−1.85	...
3435	J010832.07+150122.9	0.0414	33	0.25	8.97	−1.79	...
3508	J011900.04+143643.1	0.0365	64	0.17	8.69	−1.68	*
3757	J012227.97+153238.4	0.0376	65	0.21	8.80	−1.72	*
3854	J013854.76+150117.7	0.0279	4	0.63	9.02	−1.89	...
3859	J013901.89+145808.5	0.0285	24	0.26	8.65	−1.53	*
3821	J014042.68+133304.6	0.0447	27	0.26	9.05	−1.82	...
4094	J014326.66+131913.0	0.0276	15	0.35	8.76	−1.79	...
4119	J014629.79+135709.6	0.0444	5	0.55	9.37	−1.82	*
4195	J014906.09+142550.6	0.0445	85	0.18	8.89	−1.73	...
4074	J014911.62+125111.6	0.0262	4	0.64	8.96	−2.21	...
4065	J014941.82+124458.2	0.0490	80	0.16	8.91	−1.26	...
3880	J020519.88+131530.7	0.0270	16	0.36	8.74	−1.78	*
4040	J021139.06+140830.3	0.0269	19	0.33	8.70	−1.62	*
3985	J021412.12+132612.8	0.0411	29	0.24	8.94	−1.82	...
51416	J075559.95+125853.2	0.0445	4	0.70	9.48	−1.79	...
56319	J080322.76+095745.8	0.0345	55	0.18	8.66	−1.48	*
25844	J091959.74+100631.7	0.0326	40	0.20	8.66	−1.59	*
8347	J093858.50+040940.5	0.0463	75	0.19	8.95	−1.73	...
20305	J095243.86+100001.0	0.0303	30	0.24	8.67	−1.63	...
20371	J095402.22+103629.6	0.0399	4	0.75	9.41	−1.83	*
18755	J100057.16+073743.2	0.0489	4	0.75	9.59	−1.72	...
14863	J100134.25+065555.3	0.0489	4	0.79	9.61	−1.78	...
18875	J102004.22+074622.1	0.0451	9	0.49	9.34	−1.77	*
18872	J102039.65+075133.9	0.0451	8	0.46	9.31	−1.82	*
54233	J102157.80+243918.7	0.0402	5	0.61	9.32	−1.82	*
26336	J102316.17+130528.7	0.0320	4	0.77	9.22	−1.78	*
26319	J102339.36+130227.4	0.0322	40	0.21	8.67	−1.62	...
23069	J102742.61+104927.6	0.0316	35	0.26	8.74	−1.48	...
23039	J102756.01+111444.6	0.0325	12	0.37	8.92	−1.86	...
54763	J103721.85+272131.4	0.0421	8	0.51	9.29	−1.82	*
23228	J103920.02+114128.1	0.0479	15	0.37	9.26	−1.78	*
26640	J104028.50+133721.9	0.0317	4	0.65	9.15	−1.84	...
29594	J104639.64+140647.4	0.0336	45	0.24	8.76	−1.27	...
15242	J105016.92+060721.3	0.0422	75	0.17	8.81	−1.80	...
23437	J105147.93+115901.7	0.0465	28	0.23	9.04	−1.87	*
54986	J105739.31+272937.1	0.0454	8	0.49	9.34	−1.85	*
17684	J110037.27+102613.9	0.0361	4	0.70	9.29	−1.79	...
23518	J110103.65+120827.7	0.0342	50	0.20	8.70	−1.73	...
23563	J110741.70+130132.4	0.0350	4	0.71	9.27	−1.99	*
17840	J111254.48+093050.3	0.0291	25	0.26	8.66	−1.53	*
15612	J111341.33+074545.9	0.0291	24	0.25	8.65	−1.88	...
23539	J111447.94+114735.0	0.0379	76	0.17	8.73	−1.46	...
12597	J114309.53+055557.8	0.0315	34	0.24	8.70	−1.61	...
18202	J121134.94+092106.8	0.0269	20	0.30	8.67	−1.58	...
30192	J121418.23+142345.8	0.0251	15	0.35	8.67	−1.76	...
18482	J123053.16+090456.9	0.0393	88	0.17	8.75	−1.68	*
12970	J123553.79+054539.8	0.0418	18	0.34	9.11	−1.78	*
24366	J123938.86+122507.9	0.0411	20	0.33	9.08	−1.78	*
28462	J124618.26+115224.8	0.0449	50	0.22	8.97	−1.76	*
28461	J124622.67+115235.7	0.0443	4	0.63	9.43	−1.93	*
13091	J125451.85+035305.4	0.0483	4	0.86	9.64	−1.80	*
28551	J125657.07+122148.6	0.0496	10	0.49	9.42	−1.76	*
25236	J131357.26+123533.2	0.0256	15	0.32	8.64	−1.60	...
25202	J131415.99+120348.5	0.0343	45	0.23	8.76	−1.76	...
26911	J131621.43+133006.6	0.0304	4	0.70	9.14	−1.84	...
34531	J132939.26+294612.3	0.0472	5	0.75	9.56	−1.71	...
13551	J134505.90+034815.3	0.0331	44	0.21	8.70	−1.35	...
25475	J134807.60+112405.1	0.0360	60	0.18	8.71	−1.63	...
25572	J140700.00+130019.1	0.0274	20	0.28	8.65	−1.80	*
41444	J141547.01+085436.6	0.0287	12	0.35	8.78	−1.95	*
45439	J141722.70+250310.1	0.0299	5	0.67	9.11	−1.79	...
30847	J141835.33+072118.8	0.0250	14	0.42	8.74	−1.55	*
28875	J143041.62+115913.3	0.0271	19	0.33	8.71	−1.68	...

Table A.3. continued.

GASS (1)	SDSS ID (2)	z_{SDSS} (3)	T_{on} (min) (4)	rms (mJy) (5)	Log $M_{HI,lim}$ ($M_\odot$) (6)	Log $M_{HI,lim}/M_\star$ (7)	Note (8)
9601	J143351.42+034046.1	0.0288	5	0.69	9.08	−1.75	*
29225	J144636.62+115108.7	0.0294	29	0.28	8.72	−1.68	...
38728	J145055.60+093946.5	0.0386	84	0.15	8.67	−1.41	*
10012	J145243.07+031329.3	0.0279	8	0.50	8.91	−1.85	*
10058	J145413.13+045029.5	0.0347	4	0.71	9.26	−1.80	*
39120	J150935.51+102525.9	0.0276	25	0.34	8.74	−1.52	*
38974	J151133.48+092824.2	0.0353	4	0.70	9.27	−1.90	...
10297	J151252.96+043050.4	0.0370	4	0.64	9.27	−1.87	*
39211	J151435.92+082002.1	0.0334	8	0.56	9.13	−1.90	*
42011	J151615.35+064747.5	0.0343	13	0.44	9.05	−1.73	*
42174	J151817.19+070757.0	0.0320	65	0.18	8.60	−1.74	*
46564	J151925.35+254713.6	0.0323	4	0.59	9.12	−1.93	*
39600	J152750.23+094002.2	0.0436	49	0.21	8.93	−1.79	*
10827	J220147.39+131228.5	0.0301	30	0.26	8.69	−1.42	...
10813	J220358.03+115421.2	0.0268	14	0.39	8.77	−1.78	...
10836	J220419.41+125806.2	0.0274	8	0.53	8.92	−1.77	...
10863	J220848.81+132152.9	0.0275	20	0.35	8.75	−1.73	*
10890	J221241.31+140434.4	0.0252	14	0.39	8.72	−1.63	...
10896	J221336.49+134020.7	0.0278	20	0.30	8.69	−1.44	...
10942	J221530.28+134023.4	0.0251	14	0.42	8.75	−1.29	...
10943	J221540.59+133616.9	0.0275	20	0.28	8.66	−1.57	...
10944	J221543.66+134252.3	0.0262	25	0.31	8.66	−1.39	...
10950	J221559.51+132715.3	0.0254	14	0.44	8.78	−1.43	...
10949	J221600.51+130851.8	0.0262	19	0.33	8.68	−1.65	...
10948	J221636.89+131514.4	0.0258	40	0.24	8.53	−1.49	...
10953	J221652.39+132533.5	0.0256	16	0.34	8.67	−1.54	...
10952	J221657.95+133235.0	0.0262	19	0.31	8.65	−1.82	*
10879	J221750.25+125941.7	0.0360	59	0.19	8.72	−1.33	*
10979	J221859.40+131114.8	0.0268	18	0.31	8.68	−1.65	*
11041	J224237.97+132844.5	0.0373	72	0.18	8.73	−1.30	...
11087	J225525.96+125539.3	0.0376	14	0.45	9.13	−1.75	*
11132	J230146.58+133218.8	0.0341	29	0.27	8.83	−1.79	...
11267	J231142.06+150638.2	0.0400	8	0.49	9.23	−1.84	*
11280	J231530.93+134040.6	0.0400	10	0.40	9.14	−1.85	...
11397	J232447.10+142301.6	0.0395	90	0.14	8.67	−1.79	*
11366	J232621.83+141230.1	0.0430	23	0.30	9.08	−1.79	*
11357	J232624.38+135742.9	0.0433	24	0.26	9.03	−1.84	*
11582	J232748.74+142831.1	0.0411	20	0.35	9.10	−1.76	*
11770	J234646.15+160235.0	0.0416	4	0.66	9.39	−1.92	...
11754	J234823.35+143004.8	0.0409	28	0.28	9.01	−1.76	...
11783	J235224.35+143535.1	0.0270	19	0.31	8.68	−1.65	...

Appendix B: Notes on individual objects

We list here notes for galaxies marked with an asterisk in the last column of Tables A.2 and A.3. The galaxies are ordered by increasing GASS number. In what follows, AA2 is the abbreviation for ALFALFA detection code 2.

Detections (Table A.2)

3189 – small blue smudge 20 arcsec NW, perhaps responsible for asymmetric HI profile? AA2.
3439 – AA2.
3465 – AA2.
3509 – RFI spikes at 1350 and 1352.2 MHz (~15100 and 15500 km/s); small galaxy ~2 arcmin S has $z = 0.122$, no contamination problems.
3519 – superposed on early type galaxy without z: galaxy pair or superposition effect? Disk galaxy ~1 arcmin E has $z = 0.0597$, no contamination problems. Stronger in polarization A but OK (polarization B has noisy baseline).
3918 – low frequency edge uncertain, systematic error.
3977 – AA2.
3981 – stronger in polarization A.
4030 – there seems to be a hint of signal from another galaxy at 1358-59 MHz (~13700 km/s, no RFI there). Perhaps the small red galaxy ~1.5 arcmin SW? There are two other galaxies, even smaller or farther away.
4038 – high frequency edge uncertain, systematic error.
4039 – blue companion ~1.7 arcmin E ($z = 0.0260$, 1384.41 MHz); another blue galaxy ~1.5 arcmin SW has $z = 0.081$, no contamination problems; AA2.
4048 – boards centered at wrong frequency by mistake.
4057 – 275 mJy continuum source 1.5 arcmin away, standing waves; high frequency edge uncertain, systematic error; AA2.
4137 – low frequency edge uncertain, systematic error. Small galaxy ~1 arcmin S has $z = 0.155$, no contamination problems.
4145 – notice small blue galaxy attached to GASS 4145, no redshift from SDSS, perhaps partly responsible for asymmetric profile (which is also not well centered on SDSS redshift). Companion galaxy ~3 arcmin SW, SDSS J015509.55+125746.1 ($z = 0.032774$, 1375.33 MHz) not detected on the side away from GASS 4145, thus unlikely to contribute to the HI signal.
4223 – several galaxies within ~3 arcmin and with SDSS redshift, all with $z > 0.08$ except SDSS J015717.50+144327.2 (disk galaxy ~1.5 arcmin SE, $z = 0.027101$, 1382.93 MHz) and SDSS J015705.49+144256.0 (small galaxy ~2.5 arcmin SW, $z = 0.025304$, 1385.35 MHz). In both cases, no HI emission is detected in the half side that is moving away from GASS 4223, thus significant contamination is unlikely. Uncertain profile; AA2.
4233 – confused: two blue companions with the same redshift (SDSS J015710.06+145500.9, ~1 arcmin SE and SDSS J015708.74+145247.4, ~3 arcmin S).
5035 – high frequency edge uncertain, systematic error.
6749 – small blue companion ~40 arcsec SW, SDSS J130748.37+031057.1, $z = 0.0378$ (1368.67 MHz), some contamination certain (notice that higher peak on the low velocity side is centered on the companion).
7520 – high frequency edge uncertain, systematic error. Stronger in polarization A. Small blue companion ~3 arcmin N (SDSS J143318.34+024205.0, $z = 0.028104$, 1381.58 MHz).
9585 – two very small companions within ~1.5 arcmin, one has the same z (0.0336), the other has $z = 0.0298$ (1379.30 MHz) and is not detected.
10831 – galaxy group: there are five galaxies within 3 arcmin E of GASS 10831, three of which with redshift $z = 0.026$, one with redshift $z = 0.029669$ and the largest one without redshift from SDSS. Very broad HI profile is likely blend of emission of gas from and/or between these galaxies. Uncertain profile.
10844 – most HI likely coming from very blue companion ~1 arcmin NE, same z (0.0270); other galaxy ~1 arcmin SE has $z = 0.154$.
10850 – RFI spikes above 1374 MHz (~10000 km/s).
10856 – blend with GASS 10831 (SDSS J220322.59+123857.6, $z = 0.027346$), ~2 arcmin SW.
10889 – confused with UGC 11948? UGC 11948 is ~3.5 arcmin W, no SDSS spectroscopy, but is in the S05 archive ($cz = 7960$ km s^{-1}, observed flux of 2.63 Jy km s^{-1}, $W_{50} = 343$ km s^{-1}).
10985 – RFI at 1350 MHz (~15600 km s^{-1}).
11003 – blend with GASS 11004 (SDSS J223707.71+141355.0, $z = 0.037666$, detected by ALFALFA and in the S05 archive), ~2.5 arcmin SW. Notice also blue companion ~1 arcmin SW without SDSS redshift.
11013 – high frequency edge uncertain, systematic error.
11015 – most of the signal likely comes from SDSS J223654.54+142452.0, a large, blue disk ~2 arcmin W, $z = 0.0365$ (1370.39 MHz).
11019 – stronger in polarization B.
11055 – high frequency edge uncertain, systematic error; clear detection but uncertain HI parameters.
11071 – low frequency edge uncertain, systematic error.
11120 – high frequency edge uncertain, systematic error; stronger in polarization B.
11126 – RFI at 1358.3 MHz (~13700 km/s).
11231 – AA2.
11250 – AA2.
11268 – 5 other galaxies within 3 arcmin, most at slightly smaller redshift; the largest is GASS 11267, ~1 arcmin SE ($z = 0.040047$, 1365.75 MHz, i.e. 2.3 MHz higher than GASS 11268), not clearly detected here (also targeted separately and listed as a non-detection). The bump in the baseline next to the HI profile, on the low velocity side, is most likely due to these companions, but the HI signal does not seem significantly affected.
11270 – low frequency edge uncertain, systematic error; much clearer in polarization B.
11285 – high frequency edge uncertain, systematic error.
11303 – low frequency edge uncertain, systematic error.
11314 – blend with GASS 11311 (SDSS J231229.22+135632.1, $z = 0.034137$, ALFALFA detection), ~1.5 arcmin E. Notice also GASS 11312 (SDSS J231225.99+135450.1, $z = 0.033927$), ~2 arcmin S. Low frequency edge uncertain, systematic error.
11383 – strong detection at ~1375.5 MHz in boards 3 and 4, perhaps the blue galaxy ~30 arcsec SW (SDSS J232547.39+140245.2, no redshift)? The negative peak in the baseline at 1374 MHz (~10100 km/s) is present in 4-minute pairs only, most likely due to a galaxy in the off scan (there is small blue galaxy at that position without SDSS redshift). AA2.
11462 – companion ~2 arcmin E (SDSS J231803.74+135400.8, $z = 0.040677$) possibly responsible for the enhanced peak at ~12100 km s^{-1}.
11513 – uncertain profile, marginal detection.
11514 – uncertain profile; marginal detection, stronger in polarization B. Small galaxy 20 arcsec SW, no optical redshift.
11763 – blend with blue companion, SDSS J234155.60+151345.9 ($z = 0.025333$), ~30 arcsec SW.
11808 – low frequency edge uncertain, systematic error.
11815 – Blue companion ~2 arcmin SE, SDSS J235313.68+160228.3 ($z = 0.048889$, 1354.20 MHz); notice

also blue galaxy ∼1 arcmin SE, no SDSS redshift. Confused. RFI double spike at 1351 MHz (outside galaxy profile), eight channels replaced by interpolation.
11824 – RFI spike at 1374.2 MHz (∼10000 km/s).
11834 – RFI at 1366-68 MHz (11600-11900 km s^{-1}). Blue disk ∼1 arcmin S, no redshift, contamination possible. AA2.
11845 – RFI spike at 1375 MHz (∼9800 km/s); blend, profile peaks uncertain. Blue companion, SDSS J235645.33+135216.4, ∼2 arcmin S with the same redshift, some contamination certain; notice that the companion is GASS 11774 (AGC 331022), detected in both ALFALFA and S05 archive (observed flux of 1.96 Jy km s^{-1}, cz = 10939 km s^{-1}, W_{50} = 323 km s^{-1}).
11917 – blend with blue companion, SDSS J000744.11+151013.3 (z = 0.045049), ∼1 arcmin S.
12318 – very likely blended with SDSS J111440.82+040039.8 ∼1 arcmin SW, z = 0.040675 (1364.89 MHz); perhaps hint of HI from another companion ∼1 arcmin SE, SDSS J111447.92+040058.6, with z = 0.038769 (1367.89 MHz, ∼11600 km/s).
13158 – profile peaks uncertain. Three small galaxies within ∼1.5 arcmin: two with redshifts close to that of GASS 13158 (z = 0.0400 and 0.0401, which are displaced enough from the target that should be visible if detected), and one without optical z; AA2.
15151 – AA2.
15166 – 1.4 Jy continuum source at 6.5 arcmin and 26 mJy at 1 arcmin, standing waves, poor baseline fit.
15211 – early-type companion ∼2 arcmin E, strong contamination unlikely.
18087 – Three galaxies within 4 arcmin and with SDSS redshifts are in the background.
18673 – two small blue galaxies within 1 arcmin, no SDSS redshift; two galaxies at ∼2.5 arcmin S and SW have z = 0.08.
18681 – detected blue companion in board 4, ∼1395.3 MHz: UGC 5308, 2 arcmin N, z = 0.017872 from NED (1395.47 MHz). Small disk galaxy ∼1 arcmin N, SDSS J095323.73+075113.7 (z = 0.039586), unlikely to contaminate HI signal.
18686 – UGC 5304, blue galaxy pair, ∼2 arcmin NE (one of the two galaxies, SDSS J095310.37+075224.8, has z = 0.0407, the other has no redshift in SDSS), some contamination certain.
18702 – the galaxy ∼1.5 arcmin W has z = 0.097. A few small galaxies without SDSS redshift within 1 arcmin, one of which is likely responsible for the narrow spike within the HI profile.
18707 – AA2.
18798 – high frequency edge uncertain, systematic error. Marginal detection. Small galaxy 80 arcsec E, SDSS J101334.44+075423.7, z = 0.045321 (1358.82 MHz). Notice asymmetric light distribution of GASS 18798 opposite to companion. Two other small galaxies within 2 arcmin have z = 0.162. Clearer in polarization B.
18862 – blue companion ∼1.5 arcmin S, offset by 0.8 MHz in frequency (SDSS J102241.78+081833.0, z = 0.045199, 1358.98 MHz), does not appear to contaminate the HI signal significantly; also notice companion ∼3 arcmin N (SDSS J102236.67+082237.8, z = 0.044278, 1360.18 MHz).
20292 – AA2.
20448 – detected also blue companion, ∼2 arcmin NW (SDSS J095808.05+110832.2, z = 0.030958).
23026 – two companions (SDSS J102726.74+110543.9, ∼1.5 arcmin NE, z = 0.032848 and SDSS J102714.26+110340.0, ∼2 arcmin SW, z = 0.032969), some contamination possible. Detected another companion centered at cz ∼8700 km s^{-1} and without SDSS redshift, perhaps SDSS J102715.87+110518.0 (small and blue, strong UV emission, ∼1.5 arcmin NW)?
23757 – profile edges uncertain, systematic error.
24437 – blend with blue companion, SDSS J123946.66+133159.8 (z = 0.046494), ∼1 arcmin SW. High frequency edge uncertain, systematic error.
25296 – profile peaks uncertain.
26639 – high frequency edge uncertain, systematic error. Signal present in both polarizations, but with different shape. Blue companion ∼2.5 arcmin NE, SDSS J104055.84+134823.1 (z = 0.032261, 1376.01 MHz), does not appear to be detected.
27167 – profile peaks uncertain. Galaxy ∼1 arcmin SE has z = 0.018, no contamination problems.
28482 – blend: blue companion ∼2.5 arcmin E, SDSS J124317.30+111241.5 (z = 0.027649, 1382.19 MHz), and small blue satellite connected to GASS 28482 certainly contributing to the HI signal.
29555 – small blobs around without SDSS redshift.
29892 – blend with SDSS J112941.76+151851.3, very blue companion ∼1.5 arcmin SW (z = 0.037872, 1368.58 MHz). Notice two other galaxies at ∼3.5 arcmin with very similar redshift. AA2.
30854 – small, almost face-on blue companion ∼2.5 arcmin SW (z = 0.024564, 1386.35 MHz) not detected. **38538** – RFI spike at 1372 MHz (∼10500 km s^{-1}).
38706 – galaxy pair (UGC 9561/Arp 173), both galaxies are blue and morphologically disturbed; blend; profile edges uncertain.
38732 – high frequency edge uncertain, systematic error. Marginal detection. Companion galaxy ∼1.5 arcmin SSW, SDSS J145030.45+093626.5 (z = 0.050193, 1352.52 MHz), has a warped disk. Some contamination almost certain. Notice another two, smaller galaxies ∼3 arcmin from GASS 38732 with approximately the same redshift.
38923 – detected companion? The feature at 1358 MHz (∼13800 km s^{-1}) is real, and could be part of the HI profile of the blue galaxy ∼4 arcmin SE (SDSS J145806.23+105716.3, z = 0.045451, 1358.65 MHz); there is also a small blue galaxy ∼2 arcmin SW, (SDSS J145751.90+105917.8, without redshift.
40260 – RFI spike at 1372 MHz (∼10500 km s^{-1}). Likely blend with SDSS J135836.27+132858.6, a large disk galaxy ∼2.5 arcmin E, z = 0.039954 (1365.84 MHz; but SDSS fiber is not centered on the galaxy). Stronger in polarization A.
40425 – AA2.
41303 – confused/blend with blue companion, SDSS J140749.05+094919.2 (z = 0.037381, 1369.22 MHz), a distorted spiral ∼2 arcmin E.
41783 – uncertain profile, systematic error; AA2.
41793 – marginal detection but well centered on SDSS redshift. Possible contamination from small companion ∼2 arcmin N (SDSS J145843.76+080057.6, z = 0.037874, 1368.57 MHz); also small galaxy ∼25 arcsec N, SDSS J145840.87+075926.9, might be merging with GASS 41793.
42287 – Small companion ∼1.5 arcmin SE (SDSS J154251.89+245826.3, z = 0.033691), marginal contamination possible; blue galaxy ∼1.5 arcmin NW has z = 0.070.
44846 – companion 2 arcmin N (z = 031119) is an elliptical galaxy, contamination unlikely; blue disk ∼2.5 arcmin NE (z = 0.028982, 1380.40 MHz) not detected. AA2.
46068 – tiny companion 2 arcmin N, SDSS J143709.19+251658.5, z = 0.034017.
51190 – high frequency edge uncertain, systematic error. Small blue galaxy ∼1 arcmin E, no SDSS redshift, perhaps responsible for this very asymmetric HI profile? Three galaxies ∼2 arcmin W of GASS 51190 all have $z > 0.07$.

56304 – AA2.
56632 – uncertain profile; companion galaxy ∼3 arcmin E, SDSS J090450.16+133342.8 (z = 0.028346, 1381.25 MHz), might contribute some signal.
57099 – RFI spike at 1352.2 MHz (∼15100 km s^{-1}). Disturbed optical appearance, likely merging; blue companion ∼2.5 arcmin W, SDSS J104210.89+152136.1 (z = 0.048828, 1354.28 MHz), unlikely to contaminate signal significantly.

Non-detections (Table A.3)
3508 – detected companion, SDSS J011907.98+143555.6, ∼2 arcmin E (z = 0.037748, 1368.74 MHz).
3757 – RFI spikes above 1373.5 MHz (below ∼10300 km s^{-1}).
3859 – ∼20 arcsec from a spiral galaxy, no redshift in SDSS. Perhaps hint of signal centered at 1380.2 MHz.
3880 – early type galaxy ∼1 arcmin E, similar redshift (z = 0.0259).
4040 – detected companion (group?), cz ∼7900 km s^{-1}. There are a few small galaxies within 2 arcmin without SDSS redshift. Notice that NED lists a galaxy group (USGC U109) 2.7 arcmin away, whose redshift is compatible with the detection (z = 0.026055, 1384.34 MHz).
4119 – the feature at 13000 km s^{-1} is well centered on the blue companion ∼2 arcmin S (SDSS J014632.27+135530.2, z = 0.043488, 1361.21 MHz), but the galaxy is clearly detected only in polarization A.
9601 – group: two companions with z = 0.0330 (1375.03 MHz; 20 arcsec N, blue disk) and z = 0.0307 (1378.10 MHz; ∼1 arcmin SW) also not detected. Blue spiral ∼2 arcmin SE has z = 0.146.
10012 – marginal detection? Signal most likely dominated by edge-on disk ∼2.5 arcmin E, z = 0.0282 (1381.45 MHz; GASS 10012 has z = 0.0279).
10058 – galaxy pair.
10297 – negative feature at 1365 MHz (∼12100 km s^{-1}) is not RFI and is present in both polarizations.
10863 – marginal detection? Notice also blue companion ∼3 arcmin NE, SDSS J220857.85+132404.0 (z = 0.027224, 1382.76 MHz) that might contribute to marginal signal.
10879 – RFI spike at 1375 MHz (far from galaxy), four channels replaced by interpolation.
10952 – near bright star.
10979 – detected blue companion, SDSS J221900.09+131019.1, ∼1 arcmin S (z = 0.027923, 1381.82 MHz).
11087 – RFI spikes above 1374 MHz (below ∼10100 km s^{-1}).
11267 – companion of GASS 11268 (see detections), marginally detected here (between 12300 and 12700 km/s); four additional companions within 3 arcmin, one of which is connected to 11267 by a stellar bridge. The peak at ∼12150 km s^{-1} might be due to SDSS J231137.64+150443.8, a galaxy ∼2 arcmin SW with z = 0.040764 (1364.77 MHz).
11357 – detected blue, irregular companion ∼1 arcmin NW, SDSS J232620.87+135857.0 (z = 0.043973, 1360.58 MHz).
11366 – detected blue companion ∼1 arcmin SW, SDSS J232618.72+141150.5 (z = 0.041754, 1363.48 MHz).
11397 – near bright star; detected blue companion ∼2.5' SE, SDSS J232453.13+142059.5 (z = 0.040886, 1364.61 MHz).
11582 – detected companion in board 4, ∼1377.5 MHz: perhaps SDSS J232751.00+142820.8, very blue gal. ∼40 arcsec E without redshift?
12002 – RFI spike at 1375 MHz (∼9900 km s^{-1}).
12005 – blue companion ∼2 arcmin SW (SDSS J002416.73+144505.9, z = 0.030938, 1377.78 MHz) also not detected.
12970 – galaxy group; GASS 12967 is 2 arcmin N, same redshift; marginally detected companion ∼1 arcmin SE, z = 0.0412 (1364.20 MHz)?
13091 – blue galaxy ∼80 arcsec W has z = 0.040424, well away from GASS 13091.
17840 – detected blue companion in board 4, ∼1391.5 MHz: SDSS J111250.15+093139.1, ∼1 arcmin W, z = 0.020879 (1391.36 MHz).
18482 – detected blue companion, SDSS J123056.18+090548.9 (z = 0.038956, 1367.15 MHz), ∼1 arcmin NE.
18872 – red companion (SDSS J102034.04+075106.5, ∼1.5 arcmin W, z = 0.044115) also not detected.
18875 – three small companions within 2-4 arcmin also not detected.
20371 – detected blue companion ∼1.5 arcmin E (SDSS J095407.95+103625.6, z = 0.040392).
23228 – companion ∼1.5 arcmin SE, same redshift.
23437 – detected blue, irregular companion ∼2 arcmin SW, SDSS J105144.24+115735.4 (z = 0.046049, 1357.88 MHz), but stronger in polarization B.
23563 – small companion ∼2.5 arcmin S.
24366 – hint of detection? It would be a 3.1 sigma detection, dubious. Companion galaxy ∼1.5 arcmin NW (GASS 24364, SDSS J123936.04+122619.9, z = 0.040856) has a very disturbed morphology. Notice another galaxy ∼4 arcmin NE with similar redshift (SDSS J123951.16+122646.8, z = 0.040727).
25572 – detected blue, asymmetric companion ∼80 arcsec E, SDSS J140705.05+130013.3 (z = 0.027756, 1382.05 MHz). The small peak at 8000 km s^{-1} is present in polarization A only.
25844 – marginally detected companion, SDSS J091951.55+100812.9 ∼2.5 arcmin NW (z = 0.033534, 1374.32 MHz).
26336 – RFI spike at 1372 MHz (∼10500 km s^{-1}). Two companions within 3 arcmin.
28461 – galaxy pair: the companion is GASS 28462, ∼1 arcmin W, also not detected.
28462 – galaxy pair: the companion is GASS 28461, ∼1 arcmin E, also not detected.
28551 – RFI spike at 1352.2 MHz (∼15100 km s^{-1}). Small companion ∼1 arcmin SW, same redshift.
30847 – hint of detection? It would be a 3.8 sigma detection, dubious. Large galaxy ∼1.5 arcmin NE (SDSS J141838.81+072238.4, z = 0.025667, 1384.86 MHz) not detected.
38728 – detected companion without SDSS redshift? Optical counterpart not obvious, perhaps SDSS J145052.31+094028.0 (∼1 arcmin NW)?
39120 – hint of detection?
39211 – hint of detection?
39600 – GASS 39567, detected in DR1, is ∼2.5 arcmin S, different redshift (z = 0.031); blue galaxy ∼2 arcmin NW is in the foreground (z = 0.006).
41444 – marginally detected companion, a spiral galaxy ∼2 arcmin SW, SDSS J141541.05+085318.4 (z = 0.02942, 1379.81 MHz), but signal is visible in polarization B only; notice also two early-type galaxies within 2 arcmin, no redshifts.
42011 – detected companion, perhaps SDSS J151618.38+064812.9 (∼1 arcmin NE) or SDSS J151609.56+064741.7 (small and blue, ∼1.5 arcmin W), both without SDSS redshifts. Two other galaxies within 3 arcmin have redshifts that do not match the HI detection (SDSS J151610.69+064640.8, z = 0.033492 and SDSS J151618.58+064517.6, z = 0.035204).
42174 – edge-on disk ∼2.5 arcmin NE (z = 0.033545, 1374.30

MHz) also not detected.
46564 – it looks like a marginal detection, but the signal is in polarization A only, and is not well centered on the SDSS redshift; also galaxy has a low inclination, not consistent with wide profile.
54233 – companion 2 arcmin N.
54763 – small galaxy ∼2 arcmin SE ($z = 0.045834$, 1358.16 MHz) also not detected; small galaxies without SDSS redshift nearby.
54986 – companion (SDSS J105734.98+273020.4, $z = 0.04595$, 1358.01 MHz) ∼1 arcmin NW also not detected.
56319 – near bright star.